HHS Public Access

Author manuscript

Cell Rep. Author manuscript; available in PMC 2020 August 10.

Published in final edited form as:

Cell Rep. 2020 June 30; 31(13): 107834. doi:10.1016/j.celrep.2020.107834.

Zeb2 is a regulator of astrogliosis and functional recovery after CNS injury

Ana L. Vivinetto[1,7], **Il-doo Kim**[1,7], **David C. Goldberg**[1], **Lilah Fones**[1], **Elizabeth Brown**[1], **Victor S. Tarabykin**[3,4], **Caitlin E. Hill**[1,2,5], **Sunghee Cho**[1,2], **John W. Cave**[1,2,6,8,*]

[1]Burke Neurological Institute, 785 Mamaroneck Avenue, White Plains, NY, 10605, USA

[2]Feil Family Brain and Mind Research Institute, Weill Cornell Medicine, 1600 York Avenue, New York, NY, 10065, USA

[3]Institute of Cell Biology and Neurobiology, Charité - Universitätsmedizin Berlin, Charitéplatz 1, 10117 Berlin, Germany

[4]Lobachevsky State University of Nizhny Novgorod, Gagarina Ave 23, 603950 Nizhny Novgorod, Russia

[5]Neural Stem Cell Institute, One Discovery Drive, Rensselaer, NY 12144, USA

[6]Department of Chemistry and Life Science, United States Military Academy, West Point, NY, 10996, USA

[7]These authors contributed equally

[8]Lead contact

Summary

The astrocytic response to injury is characterized on the cellular level, but our understanding of the molecular mechanisms controlling the cellular processes is incomplete. The astrocytic response to injury is similar to wound healing responses in non-neural tissues that involve epithelial-to-mesenchymal transitions (EMT) and an upregulation in ZEB transcription factors. Here we show that injury-induced astrogliosis increases EMT-related genes expression, including the *Zeb2,* as well as long non-coding RNAs, including *Zeb2os,* which facilitates ZEB2 protein translation. In mouse models of either contusive spinal cord injury or transient ischemic stroke, the conditional knockout of *Zeb2* in astrocytes attenuates astrogliosis, generates larger lesions, and delays recovery of motor function. These findings reveal ZEB2 as an important regulator of the astrocytic

[*]*Lead Contact and Corresponding Author Information:* John W. Cave, Burke Neurological Institute, Weill Cornell Medicine, 785 Mamaroneck Avenue, White Plains, NY, 10605, Phone: 914-368-3140, Fax: 914-597-2757, joc2042@med.cornell.edu.

Author Contributions

ALV, CEH, SC, and JWC conceived and designed experiments. ALV, IK, DCG, LF, EB, CEH, and JWC performed experiments and analyzed data. ALV, IK, DCG, CEH, SC, and JWC drafted and edited manuscript. VST provided essential reagents, technical advice, and manuscript review.

Declaration of Interests

The authors declare that they have no competing interests related to the studies reported in this manuscript.

response to injury and suggest that astrogliosis is an EMT-like process, which provides a conceptual connection for the molecular and cellular similarities between astrogliosis and wound-healing responses in non-neural tissue.

eTOC blurb

Vivinetto et al. identify the EMT-related transcription factor ZEB2 as a regulator of the astrocytic response to injury. Mouse models of either stroke or SCI show that knock-out of *Zeb2* in astrocytes attenuates astrogliosis, increases lesion sizes, and delays recovery motor function. Together, the findings suggest that astrogliosis is an EMT-like process.

Graphical Abstract

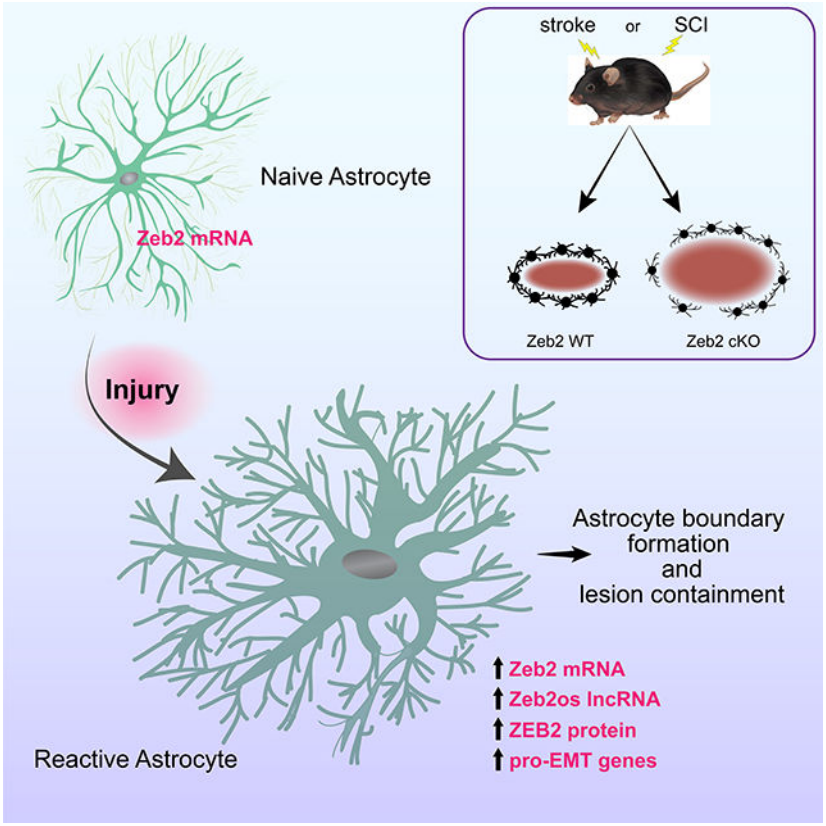

Introduction

Injury in the central nervous system (CNS) initiates astrogliosis, which is characterized by cellular changes to astrocytes that include hypertrophy and thickened processes as well as extensive changes in gene expression (Sofroniew, 2014). The scale of the astrocytic response is dependent on injury severity and distance from the lesion. After severe injuries, reactive astrocytes adjacent to the lesion organize to form a dense boundary that isolates the lesion and protects surrounding tissue from further damage. In addition to generating a physical barrier, reactive astrocytes also facilitate blood-brain-barrier repair as well as attenuate osmotic and oxidative stresses (Pekny and Pekna, 2014). Studies that either genetically

modified or ablated astrocytes have demonstrated the importance of astrogliosis and astrocyte boundary formation in protecting neurons and neurological function. These studies showed that disrupting the astrocytic response to injury increases the lesion size and worsens recovery of neurological function (Anderson et al., 2016; Bhalala et al., 2012; Brambilla et al., 2005; Bush et al., 1999; Faulkner et al., 2004; Herrmann et al., 2008; Hsu et al., 2008; Okada et al., 2006; Sahni et al., 2010; Wanner et al., 2013). Reactive astrocytes that undergo mild to moderate astrogliosis can resolve and return to their pre-injury physiology, but the boundary-forming astrocytes adjacent to the lesion maintain their reactive phenotype in the chronic phase (Sofroniew, 2014).

The astrocytic cellular response to CNS injury has several similarities with wound healing in non-neural tissue (Burda and Sofroniew, 2014; Stroncek and Reichert, 2008). Moreover, in several tissues, severe injury and inflammation can also result in fibrosis and the formation of a scar tissue boundary that resembles the chronic astrocytic boundary. The non-neural wound healing process involves epithelial cells that undergo a transition to a mesenchymal phenotype that includes extensive cytoskeletal remodeling, degrading cell-cell junctions, and altering the ECM (Haensel and Dai, 2018). This epithelial-to-mesenchymal transition (EMT) is promoted by signaling pathways, such as JAK/STAT, EGF, and TNFa (Jere et al., 2017; Stone et al., 2016; Yan et al., 2010), which also promote astrogliosis after injury (Li et al., 2011; Okada et al., 2006; Wanner et al., 2013; White et al., 2011). In addition to wound healing, EMT is also a well-studied process in development and cancer metastasis (Nieto et al., 2016). The similarities between astrogliosis and EMT suggest that the astrocyte response to injury can be modified by targeting EMT-related factors.

Zeb2 encodes a zinc-finger homeodomain transcription factor protein that has an established role in controlling cell mobility, cell adhesion, and cytoskeletal reorganization in wound healing, development, and cancer (Lamouille et al., 2014; Rogers et al., 2013; Zheng and Kang, 2014). *Zeb2* also regulates several processes in neural development, including neuroectoderm formation, alternative cell fate decisions, proliferation and differentiation (Chng et al., 2010; Dang and Tropepe, 2010; Dang et al., 2012; He et al., 2018; McKinsey et al., 2013; Miquelajauregui et al., 2007; Nitta et al., 2004; Seuntjens et al., 2009; Van de Putte et al., 2003; van Grunsven et al., 2007; Weng et al., 2012). The role for *Zeb2* in the normal or pathological adult CNS, however, is unknown. In this study, we identified a subset of EMT-related genes, which included *Zeb2,* whose expression is upregulated in astrogliosis. We explored the role of *Zeb2* in regulating the astrocytic response to injury in mouse model systems of either spinal cord injury (SCI) or ischemic stroke. These studies identify *Zeb2* as a regulator of astrogliosis and the recovery of motor function. Together, these findings provide insight into the molecular mechanisms directing the astrocytic response to injury and suggest that astrogliosis is related to wound healing processes in non-neural tissues on both a cellular and molecular level.

Results

EMT-like changes in astrocytic gene expression following injury

To identify EMT-related genes that have expression levels modified by the induction of astrogliosis following injury, we examined publicly available RNA-seq data of astrocyte

gene expression in adult mice that were either uninjured or at 14 days following a spinal cord crush injury (Anderson et al., 2016). This analysis examined a set of 181 genes combined from canonical EMT-related marker genes (Zeisberg and Neilson, 2009) and the EMT Gene Set Enrichment Analysis (GSEA) dataset for genes defining EMT in wound healing, fibrosis, and metastasis (Subramanian et al., 2005). Changes in gene expression associated with EMT include genes that have expression levels up-regulated and genes that have expression levels down-regulated. The combined dataset we examined contained 139 pro-EMT genes that are upregulated during EMT and/or promote EMT, as well as 42 EMT genes that are down-regulated during EMT and/or suppress EMT. Both pro- and anti-EMT genes broadly belonged to seven functional categories: cell-surface and adhesion proteins, cytoskeleton-associated proteins, ECM proteins, intercellular signaling proteins, transcription factors, intracellular signaling, and cellular metabolism.

Astrogliosis and EMT share several similar cellular features, but reactive astrocytes never attain a fully mesenchymal phenotype, which suggests that astrogliosis involves only a partial upregulation of pro-EMT genes. Consistent with this expectation, the expression levels for a subset of pro-EMT genes (41%, 57/139 genes) were increased in reactive astrocytes, whereas the levels for most remaining pro-EMT genes (71/83 genes) were unchanged (Supplemental Figure 1). The majority of pro-EMT genes (35/57 genes) that increased in reactive astrocytes were either ECM or cell-surface and adhesion proteins (Supplemental Figure 1). Since naïve astrocytes have only limited morphological and functional similarities to epithelial cells, only modest changes in the expression levels of EMT genes that suppress epithelial phenotypes were expected in astrogliosis. Consistent with this expectation, the expression levels for most anti-EMT genes (62%, 26/42 genes) remain unchanged in reactive astrocytes (Supplemental Figure 2), and only a small subset of anti-EMT genes (8/42 genes) was also down-regulated in reactive astrocytes (Supplemental Figure 2). Thus, despite the differences in the starting phenotypes of epithelial cells and astrocytes, our analysis indicates that EMT and astrogliosis upregulate a shared subset of genes that underlie many of the similar cellular changes that occur in both processes. Together, these findings indicate that changes in gene expression that are part of the astrocyte response to injury overlap with established changes in gene expression associated with EMT.

SCI-induced expression of ZEB1/2 in mouse astrocytes

Because the expression of a substantial subset of EMT-related genes is upregulated in astrogliosis, we expected that targeting key EMT genes could modify the induction of astrogliosis after injury. We focused on the SNAIL, TWIST, and/or ZEB transcription factors because these proteins are important regulators of gene expression in EMT (Lamouille et al., 2014). Our analysis of EMT-related genes found that spinal cord astrocytes have little or no expression of *Twist* and *Snail* family genes either before or after injury (Figure 1A). By contrast, *Zeb1/2* were expressed in both uninjured and post-SCI astrocytes, and only *Zeb2* expression levels were responsive to SCI (Figure 1A). We performed qRT-PCR assays with whole spinal cord tissue from adult C57Bl6 mice with contusive SCI and confirmed that *Zeb1* expression levels do not significantly change following injury (Figure 1B) and that *Zeb2* expression levels increase following SCI (Figure 1C). Our qRT-PCR

analysis found that the up-regulation of *Zeb2* expression peaks at 7 days post-injury and returns to baseline levels by 14 days post-injury, which contrasts with the RNA-seq data indicating that *Zeb2* levels remain elevated at 14 days post-injury *(cf* Figure 1A *vs.* Figure 1C). This discrepancy likely reflects differences in RNA isolation methods (we used whole spinal cord tissue, whereas the RNA-seq database isolated RNA from astrocytic ribosomes) and/or differences in the type of injury used to generate reactive astrocytes (spinal cord crush vs. contusion). Despite this discrepancy, the findings clearly show that the *Zeb1/2* canonical EMT transcription factor genes are expressed in naïve and reactive adult astrocytes.

To further explore the role of *Zeb1/2* in the astrocytic response to injury, we examined ZEB1 and ZEB2 protein expression in spinal cord tissue from sham-injured and 14-day post-injured mice. This immunofluorescence analysis showed that both ZEB1 and ZEB2 expression levels strongly increase after injury (Figure 1D–G). Both transcription factors are expressed in the spinal cord tissue surrounding the lesion, but ZEB1 was also strongly expressed within the lesion core, whereas ZEB2 was absent from the lesion core (Figure 1E *vs.* 1G). Further immunofluorescence analyses of ZEB1 expression in the spinal cord surrounding the lesion showed that ZEB1 is expressed in many cell types, including astrocytes (GFAP+), neurons (NeuN+), oligodendrocytes (OLIG2+), microglia/macrophages (CD11b+), and endothelial cells (CD31+)(Supplemental Figure 3). By contrast, ZEB2 expression in the spinal cord after injury was nearly exclusive to astrocytes (Figure 1H, M, R). ZEB2 expression was absent in microglia/macrophages (CD11b+; Figure 1I, N, S), endothelial cells (CD31+; Figure 1J, O, T), and neurons (NeuN+; Figure 1K, P, U), and only a small number of scattered oligodendrocytes (OLIG2+; Figure 1L, Q, V) co-expressed ZEB2. Together, these findings show that SCI induces a strong, but differential, increase in ZEB1 and ZEB2 expression levels. The induction of ZEB1 expression is broad and observed in many cell types, whereas ZEB2 was almost exclusive to reactive astrocytes. Given our focus on molecular mechanisms regulating astrogliosis, our studies hereafter concentrated on the role of ZEB2.

To better characterize the temporal changes in ZEB2 protein expression, immunofluorescence and western blots analyzed protein expression in mice at multiple time points post-SCI. At 3 days, the immunofluorescence analyses showed scattered expression at the lesion border and in the parenchyma, as well as expression in cells lining the central canal. At 7 days post-injury, however, there was wide-spread and strong expression in astrocytes surrounding the lesion as well as in white and gray matter astrocytes within the rostral and caudal territories. This expression appeared to peak between post-injury days 7 and 14, after which expression levels decreased, but remained detectable near the lesion boundary for as long as 30-days post-SCI (Figure 2A–F). Western blot analyses with whole spinal cord tissue revealed that ZEB2 was partitioned to both the cytoplasm and nucleus (Figure 2G–I). Distinct isoforms were detected in the cytoplasm and nucleus of sham-injured mice, whereas nuclear isoforms were also present in the cytoplasm post-injury. Together, these findings indicate that there is a dynamic and complex regulation of ZEB2 expression and cellular localization following injury.

SCI-induced expression of Zeb2os in astrocytes

Efficient translation of *Zeb2* mRNA into protein requires the co-expression of the *Zeb2os* long non-coding RNA (lncRNA)(Beltran et al., 2008). *Zeb2os* is a conserved lncRNA in mice and humans that is transcribed from the opposite genomic strand encoding *Zeb2* and partially overlaps with the *Zeb2* 5'-UTR (Figure 3A). Like Zeb2 and canonical markers of astrogliosis, such as *Gfap,* examination of the astrocyte RNA-seq data (Anderson et al., 2016) found that SCI induces *Zeb2os* expression in astrocytes (Figure 3B–D). qRT-PCR analyses with whole spinal cord tissue showed that *Zeb2os* levels also peaked at post-injury day 7 (Figure 3E) and *in situ* hybridization confirmed induction of *Zeb2os* in astrocytes following SCI (Figure 3F–J). STAT3 is a transcription factor that is a well-established regulator of astrogliosis and the targeted loss of *Stat3* in astrocytes diminishes astrogliosis, disrupts border formation, increases lesion size, and impairs recovery of motor function after SCI (Anderson et al., 2016; Herrmann et al., 2008; Okada et al., 2006; Wanner et al., 2013). Our analysis of the astrocyte RNA-seq data found that the SCI-induced upregulation of *Zeb2os,* but not *Zeb2,* expression, was dependent on *Stat3* (Figure 3B–D). Moreover, we found that *Zeb2os* was one of 17 lncRNAs that significantly changed their expression level following SCI, and the loss of *Stat3* in astrocytes blocks the injury-induced changes for 11 of these lncRNAs, including *Zeb2os* (Figure 3K; Supplemental Figure 4). Together, these findings suggest that the injury-induced activation of STAT3 indirectly drives ZEB2 protein expression through the up-regulation of *Zeb2os* expression.

Targeted knockout of Zeb2 in astrocytes attenuates astrogliosis

To establish whether *Zeb2* was required for astrogliosis after SCI, we conditionally deleted *Zeb2* from astrocytes of *Gfap-cre*^{ERT2}/*Zeb2*$^{flox/flox}$ adult mice. Severe injury triggers the generation of new astrocytes near the lesion (Sofroniew, 2014) and in order to ensure that astrocytes generated after injury also have *Zeb2* deleted, tamoxifen was administered for 7 continuous days starting 3 days prior to injury. At 14 days post-injury, elimination of ZEB2 expression was largely complete, with only scattered ZEB2+ astrocytes adjacent to the lesion (Supplemental Figure 5A, B).

Analysis of conditional astrocytic *Zeb2* knockout (*Zeb2*cKO) mice revealed several changes in the astrocytic response after SCI. Knockout of astrocytic *Zeb2* significantly increased the lesion size at 14days post-injury (Figure 4A–H), which was accompanied by a reduction in GFAP expression intensity (Figure 4I–L). Reconstructions of individual astrocytes in the gray matter 1mm from the lesion boundary revealed reduced hypertrophy in the primary processes of Zeb2*cKO* mice 14 days post-injury (Figure 4M–Q). By contrast, astrocytes in gray matter 3mm from the lesion boundary, where astrogliosis is less severe, showed no noticeable difference in the thickness of processes. This indicates that the differences observed at 1mm are likely due to an impaired astrocytic response in Zeb2*cKO* mice rather than Zeb2*cKO* astrocytes having general morphological changes. Together, these findings show that the induction of astrogliosis by SCI was attenuated in the Zeb2*cKO* mice and that *Zeb2* is necessary for the full astrocytic response to injury.

To establish whether *Zeb2* also regulates the astrocytic response to injury in the brain, we examined ZEB2 expression in mice after a 30-minute ischemic stroke (transient medial

cerebral arterial occlusion). Analysis of *Zeb2* and *Zeb2os* expression levels from whole brain tissue found that expression levels for both genes were increased specifically in the hemisphere ipsilateral to the infarct and these levels remain elevated for at least 14days after stroke (Figure 5A, B). Immunofluorescence analysis showed that stroke strongly induced ZEB2 expression in astrocytes in the hemisphere ipsilateral to the infarct (Figure 5C–G), suggesting that the induction of ZEB2 expression in astrocytes following injury is a general response in the CNS.

To address whether the targeted loss of *Zeb2* in brain astrocytes also attenuated astrogliosis and impacted the lesion size following stroke, Zeb2*cKO* mice were administered tamoxifen for the 5 days prior to stroke, but not on the day of injury or afterward because initial studies with mice receiving tamoxifen post-stroke resulted in high mortality rates. This treatment protocol also showed a knock-down, but not complete elimination, of ZEB2 from astrocytes with scattered ZEB2+ astrocytes at the lesion boundary when brains were examined 3 days post-stroke (Supplemental Figure 5C, D). Zeb2*cKO* mice had significantly larger infarct volumes and greater brain swelling relative to control mice at 3 days post-stroke, (Figure 5H–K). Immunofluorescence also showed that GFAP expression was reduced in the Zeb2*cKO* mice, consistent with the targeted knockout of *Zeb2* attenuating the astrocytic response to injury (Figure 5L, M). The exacerbated injury severity and brain swelling in Zeb2*cKO* mice were also accompanied by a significant increase IgG+ area and intensity, which indicated a profoundly larger disruption of the blood-brain-barrier (Figure 5N–Q). In addition, FITC-dextran injections also revealed enhanced vascular permeability in the ipsilateral hemisphere of Zeb2*cKO* mice following stroke (Figure 5R–U). Together, these findings show that the astrocytic response in *Zeb2cKO* mice was attenuated following stroke and accompanied by increased lesion sizes and disruptions of the blood-brain-barrier.

Impaired motor recovery in Zeb2cKO mice

To address whether the knockout of *Zeb2* in astrocytes impacted the acute recovery of function following injury, motor and reflex skills of *Zeb2cKO* and control mice were evaluated with a modified neurological severity score at both 1- and 3-days post-stroke (Li et al., 2000)(Figure 6A–C). At both time points, *Zeb2cKO* mice scored significantly worse than control mice and neither group significantly improved between 1- and 3-days post-stroke. *Zeb2cKO* mice had poorer performances on placement and proprioceptive tests, suggesting increased sensory deficits as compared to control mice. *Zeb2cKO* mice also had an increased tendency to circle towards the paretic side and were more likely to have an inability to walk in a straight line, indicating increased motor impairment. By contrast, both *Zeb2cKO* and control mice showed similar motor performance on balance beam tests and had similar reflexes to auditory or touch sensory inputs. Together, the increased overall sensory and motor impairment in *Zeb2cKO* mice was consistent with these mice experiencing larger lesions and more severe stroke-related injury than control mice.

To address whether sub-acute recovery of motor function following injury was also impacted by the knockout of *Zeb2* in astrocytes, motor function was examined in mice following contusive SCI. In general, Zeb2*cKO* mice showed a slower recovery of motor function. At post-injury day 4, 2 out of 9 control mice and 6 out of 11 Zeb2*cKO* mice dragged both

hindlimbs either with no or slight ankle flexion. By post-injury day 6, all control mice were stepping with at least one hindlimb, whereas 3 Zeb2*cKO* mice continued to drag both hindlimbs with a range of ankle flexion. All control mice had at least occasional plantar stepping on hindlimbs by post-injury day 8, but it took 12 days post-SCI for all *Zeb2cKO* mice to also show at least occasional plantar stepping with the hindlimbs. This overall pattern suggested that the recovery of motor function was delayed in Zeb2*cKO* mice.

The recovery of motor function in SCI mice was also examined by automated quantitative gait analysis (CatWalk) every other day from 4 to 14 days after injury (Figure 6D). Step sequence pattern analysis showed that prior to injury mice used either alternate or cruciate stepping sequences, but not rotate sequences (Figure 6E). After injury, however, both control and Zeb2*cKO* mice had a preference for alternate step sequences and also began using rotate sequences (Figure 6E). There was no significant preference for any step sequence pattern between control and Zeb2*cKO* mice, but Zeb2*cKO* mice were delayed in their recovery of the regularity index (Figure 6F), which is a measure of interlimb coordination (Hamers et al., 2001). The forelimbs, but not the hindlimbs, of Zeb2*cKO* mice also maintained a significantly wider base of support at 14 days post-injury (Figure 6G, H), indicating that compensatory changes in forelimb use with Zeb2*cKO* mice persisted. Consistent with this persistent altered use of the forelimbs, the maximum contact area for both forepaws, but not hind paws, was also significantly larger after 14 days post-injury (Figure 6I,J). By contrast, swing duration and stride length gait parameters did not show significant differences between control and Zeb2*cKO* mice (Supplemental Figure 6). Together, both stroke and SCI model systems of neurological injury show that the targeted knock-down of astrocytic *Zeb2* impedes the recovery of motor function after injury.

Discussion

These studies identified *Zeb2* as an important regulator of astrogliosis after both stroke and SCI. The targeted knock down of *Zeb2* in astrocytes attenuates astrogliosis, increases lesion size, and impairs recovery of motor function. Together, these findings indicate that a key role for *Zeb2* in the astrocytic response to injury is to promote astrogliosis and preserve neurological function.

The full effect of the targeted loss of astrocytic *Zeb2* is likely underestimated in this study because the knock-out of *Zeb2* in astrocytes was not complete. Previous studies that genetically modified astrocytes have typically used constitutive promoters, such as *Gfap,* to drive recombination because the loss of the target genes did not noticeably disrupt neural development (Anderson et al., 2016; Brambilla et al., 2005; Okada et al., 2006; Sahni et al., 2010; Wanner et al., 2013; White et al., 2011). By contrast, *Zeb2* has established developmental roles in the nervous system (Epifanova et al., 2019; Hegarty et al., 2015; McKinsey et al., 2013; Miquelajauregui et al., 2007; Van de Putte et al., 2003), and a previous study that deleted *Zeb2* with constitutively active CRE recombinase expressed under the control of a *Gfap* promoter reported the onset of severe tremors and defects in balance control approximately two week after birth (He et al., 2018). In order to prevent disrupting nervous system development and avoid defects that could confound our studies to address the astrocytic response in the adult nervous system, we relied on conditional

tamoxifen-driven recombination to knock-out *Zeb2* in astrocytes. This inducible system, eliminated most, but not all, ZEB2-expressing astrocytes following either SCI or stroke. This system, however, also did not produce either tremors or balance deficits in mice after receiving tamoxifen prior to injury.

The origin of ZEB2-expressing astrocytes at the lesion border in *Zeb2cKO* mice is unclear. These ZEB2-expressing astrocytes may have been generated after the final tamoxifen administration. Alternatively, or in addition, since the specific cell type responsible for post-injury astrocyte production is not established, the ZEB2-expressing astrocytes at the lesion boundary may have been derived from non-Gfap-expressing cells that were able to escape tamoxifen-induced recombination and *Zeb2* deletion. In the adult brain, some astrocytes generated following stroke are derived from progenitors in the subventricular zone (SVZ) adult neurogenic niche (Benner et al., 2013; Carlen et al., 2009; Faiz et al., 2015). Thus, some ZEB2-expressing astrocytes near the stroke lesion in our Zeb2*cKO* mice were possibly generated from proliferative transit-amplifying cells in the SVZ. These proliferative cells do not express GFAP (Mamber et al., 2013) and would not contain active CRE recombinase following tamoxifen administration, which would prevent their progenitors from being Zeb2*cKO* cells. SVZ-derived astrocytes require several days to migrate and reach cortical lesion boundaries (Benner et al., 2013; Faiz et al., 2015), however, which suggests that local proliferative cells may also contribute to the ZEB2-expressing astrocytes near the lesion we observed only 3 days after stroke in our *Zeb2*cKO mice. In the adult spinal cord, ependymal cells are a reported source of neural stem cells after injury that can generate several cell types, including astrocytes (Barnabe-Heider et al., 2010; Johansson et al., 1999; Meletis et al., 2008; Sabelstrom et al., 2013). Others have reported, however, that ependymal cells generate astrocytes only after severe injury associated with damage to the ependymal layer, but even in these cases, the contribution to post-injury astrocyte production was minimal (Ren et al., 2017). Future studies using lineage tracing will be required to unambiguously identify the origin, or origins, of these cells.

The regulatory role for ZEB2 in the astrocytic response to injury enhances our understanding of molecular mechanisms that underlie the cellular processes shared between astrogliosis and wound healing in other tissues (Burda and Sofroniew, 2014; Stroncek and Reichert, 2008). *Zeb2* was identified as part of a subset of EMT-related genes upregulated in astrocytes following injury. This subset also includes many genes encoding cell-surface, cell-adhesion, cytoskeletal, ECM, as well as inter- and intracellular signaling proteins, that together are integral for the cytoskeletal reorganization, modification of cellular junctions, tissue remodeling, and deposition of ECM components that occur in both astrogliosis and wound healing. Together, these molecular and cellular similarities strongly suggest that the induction of astrogliosis is an EMT-like process.

Viewing astrogliosis as an EMT-related process provides a conceptual connection for the molecular and cellular similarities to wound-healing responses in other tissues, as well as events in development and cancer. Astrogliosis and EMT are both generally reversible processes, although the starting and ending cellular phenotypes in astrogliosis do not correspond to the epithelial and mesenchymal cell types associated with canonical EMT in other tissues. EMT is not a completely binary process, however, and cells with partial-EMT

phenotypes are common, including in wound healing (Nieto et al., 2016). Our finding that a subset of canonical EMT genes is upregulated in reactive astrocytes is consistent with astrogliosis representing a partial EMT-process. In glioblastoma multiforme, the transformation of astrocytoma cells into an invasive phenotype is also an EMT-like process, but to reflect the differences with canonical EMT, the transformation of astrocytoma cells has been labeled a glial-to-mesenchymal transition (GMT)(Mahabir et al., 2014). Similarly, since reactive astrocytes are distinct from GBM cells as well as mesenchymal cells in canonical EMT processes, we propose labeling the underlying EMT-like process in astrogliosis an Astrocyte-to-Reactive Astrocyte Transition (ARAT).

Our findings reveal ZEB2 as a key driver of ARAT and astrogliosis, but ZEB1 co-expression in some astrocytes may partially compensate when *Zeb2* is knocked down. ZEB1/2 proteins have substantial homology, but they are not functionally redundant and germ-line knockouts of either *Zeb1* or *Zeb2* are lethal with different timing and phenotypes for each genotype (Takagi et al., 1998; Van de Putte et al., 2003). Moreover, there are also significant differences in protein-protein interactions and gene expression patterns (Vandewalle et al., 2009). In this study, both ZEB1/2 expression levels were upregulated following injury, but ZEB1 was expressed in a wide range of cell types, including astrocytes, oligodendrocytes, neuron, microglia/macrophages, and endothelial cells, whereas ZEB2 was restricted to astrocytes. This differential expression suggests that ZEB2 is part of an astrocyte-specific response, whereas ZEB1 may be part of general injury response in many cell types and is not specifically required for ARAT and astrogliosis.

Injury-induced ZEB2 expression in the adult CNS is complex and is possibly regulated at several levels. ZEB2 protein levels were low in uninjured tissue, despite the expression of *Zeb2* mRNA, but consistent with the regulation of its translation in cancer cells (Beltran et al., 2008), ZEB2 protein levels increased following injury with the induction of *Zeb2os* lncRNA expression. *Zeb2os* was identified as one of several astrocytic lncRNAs that have expression levels significantly altered following injury, which suggests that lncRNAs likely have several pivotal roles in directing the astrocytic response to injury. Our findings also show low levels of ZEB1 protein expression in uninjured tissue despite *Zeb1* mRNA expression, and a strong upregulation of ZEB1 levels following injury. In humans, like *Zeb2os,* the lncRNA *Zeb1-AS* is also expressed from the genomic strand opposite to *Zeb1* and promotes ZEB1 translation (Zhao et al., 2019), suggesting that both ZEB1/2 have similar lncRNA-mediated post-transcriptional regulatory mechanisms. In mice, however, *Zeb1-AS* has not been characterized and underscores our limited understanding of lncRNAs and their function in reactive astrocytes and other cell types in the nervous system following injury. In many tissues, ZEB1/2 levels are also modulated by miRNA-mediated mechanisms (Abba et al., 2016), but like lncRNAs, our understanding of how miRNA levels are modified in reactive astrocytes and contribute to astrogliosis is limited.

Our findings also reveal that there are multiple ZEB2 isoforms distributed between the nucleus and cytoplasm both before and after injury. These isoforms may represent differentially spliced transcripts and/or differential post-translational modifications, including SUMOlyation and phosphorylation (Li et al., 2019; Long et al., 2005). Nuclear localization of ZEB2 is required for its role as a gene transcription regulatory factor, and its

cytoplasmic localization may reflect related interactions with SMAD transcription regulatory proteins, which also traffic in between the nucleus and cytoplasm (Hill, 2009). Alternatively or in addition, recent reports indicate that ZEB2 can also bind α-tubulin (Fouani et al., 2020), which suggests that ZEB2 may influence astrocyte cytoskeleton organization through mechanisms other than solely by regulating gene transcription.

The protective role of reactive astrocytes in the acute and sub-acute stages of recovery after injury in the nervous system, as well as their role in the chronic boundary, has led to an emerging interest in targeting these cells to improve functional outcomes from neurological injury (Becerra-Calixto and Cardona-Gomez, 2017; Gleichman and Carmichael, 2014; Liddelow and Barres, 2017; Liu and Chopp, 2016; Pekny and Pekna, 2014). To identify suitable targets and advance the development of such approaches requires a more complete knowledge of the molecular regulatory pathways directing the astrocytic response to injury. In this study, we have identified ZEB2 as an important regulator of astrogliosis after either stroke or SCI that influences lesion size and motor function recovery. Several factors and molecular pathways that trigger and sustain astrogliosis have been identified (Sofroniew, 2009), but nearly all of these factors and pathways function in several cell types after injury. ZEB2, however, appears to be an astrocyte-specific factor and may provide opportunities to selectively target reactive astrocytes following injury in order to improve neuroprotection and recovery of neurological function.

STAR Methods

RESOURCE AVAILABILITY

Lead Contact—Further information and requests for resources and reagents should be directed to and will be fulfilled by the Lead Contact, John Cave (joc2042@med.comell.edu).

Materials Availability—This study did not generate new reagents or mouse lines.

Data and Code Availability—This study did not generate any code and the datasets analyzed are publicly available.

EXPERIMENTAL MODEL AND SUBJECT DETAILS

Animals—*Zeb2*^{flox} mice were rederived by the Mouse Genetics Core Facility at Weill Cornell Medicine from cryopreserved sperm purchased from the Riken Institute (stock number RBRC01924). The generation of the *Zeb2*^{flox} mice has been previously described (Higashi et al., 2002). The *Zeb2*^{flox} mice were crossed with the *Gfap-cre*^{ERT2} mouse line purchased from Jackson Labs (stock number 012849). Generation of this *Gfap-cre*^{ERT2} line has been previously described (Ganat et al., 2006). All mice, including C57BL/6J mice (Jackson Labs stock number 000664), were housed in humidity-controlled cages at 22°C under a 12:12 h light/dark cycle and provided with food and water ad libitum. All studies adult mice (3–4mo) of both sexes that weighed approximately 25g. Mice were randomly assigned to experimental groups. All procedures were carried out under protocols approved by the Weill Cornell Medicine Institutional Animal Care and Use Committee and conformed to NIH guidelines.

METHOD DETAILS

Gene Expression Analysis—All gene expression changes in reactive astrocytes relative to uninjured astrocytes were determined using publicly available RNA-seq data of astrocyte gene expression from uninjured and 14-day post-SCI adult mice (Anderson et al., 2016). This database contains gene expression information using spinal cord astrocyte-specific ribosome-associated RNA isolated from mice 2 weeks after either SCI or laminectomy. The set of 181 EMT-related genes analyzed in this study was generated by combining canonical EMT genes (Zeisberg and Neilson, 2009) and genes listed in GSEA Hallmark Epithelial-Mesenchymal Transition dataset (M5930) for EMT in wound healing, fibrosis, and metastasis (Subramanian et al., 2005). For the separate analysis lncRNA expression levels, a set of 50 lncRNAs were identified in the literature as either having expression levels that were either responsive to neurological injury (stroke or SCI) or involved with development. lncRNAs associated with development were included since developmentally-related pathways are involved in neuroprotective and regenerative responses to injury.

Spinal Cord Injury—Adult (3–4 mo) *Gfap-cre*^{ERT2}*/Zeb2*$^{fl/fl}$ (Zeb2cKO) and *Zeb*$^{fl/fl}$ (control) mice of both sexes that were approximately 25 g were administered tamoxifen (Sigma) by intraperitoneal IP injection at 100 mg/kg (2.5 mg in 0.1 ml of a 9:1 canola oil: ethanol mixture). Tamoxifen was delivered daily for three days prior to injury, the day of injury, and three days after injury. On the day of injury, mice were anesthetized with isoflurane (2.5%) before performing a laminectomy to remove the dorsal process of thoracic vertebrae 9 (T9) and expose the spinal cord. The lateral processes of T8 and T10 were clamped and a 50 kDyn injury was induced using the Infinite Horizon Impactor (Precision Systems & Instrumentation). The impact curve was checked for hit quality at the time of injury and the injury site was inspected for bruising before suturing the muscles closed in two separate anatomical layers and closing the skin with wound clips. Body temperature was monitored and maintained throughout the surgery using a thermo-regulated heating pad. Buprenorphine (0.05 mg/kg) was administered twice-a-day for the first two days post-surgery to alleviate pain. Lactated Ringer's solution (1 ml) was provided 1–2 times per day for the first two days post-surgery to prevent dehydration. Gentamycin (5 mg/kg) was administered once-a-day for the first 7 days post-surgery to prevent infections. Cages were placed on thermo-regulated heating pads to assist thermoregulation during the first week post-surgery. All procedures were carried out under protocols approved by the Weill Cornell Medicine Institutional Animal Care and Use Committee and conformed to NIH guidelines.

Quantitative Analysis of Gait Parameters after SCI—Recovery of motor function was evaluated using the automated CatWalk System (Noldus Inc.). Prior to recording baseline measurements, mice were allowed to adapt to the CatWalk apparatus by performing at least 3 compliant runs per day for 3 days. Pre-injury baseline values were collected on the day before the start of the tamoxifen injections (day −4) and on the fourth day of tamoxifen injections before SCI surgery (day 0). Following SCI, gait parameters were measured on days post-injury days 4, 6, 8, 10, 12, and 14. Three independent cohorts of control and Zeb2*cKO* mice were analyzed so that a total of 9 control and 11 *Zeb2*cKO mice were analyzed. Based on previously established metrics for rodents following contusive SCI (Hamers et al., 2006), analysis of gait parameters focused on the regularity index, base of

support, maximum contact area, stride length, and swing speed. Analyses of gait parameters were conducted by investigators blinded to the animal genotype. All CatWalk gait parameters were analyzed on Prism software (Graphpad Software) using repeated-measures ANOVA (a=0.05) with a Bonferroni's multiple comparisons post-hoc test (α=0.05).

Transient Ischemic Stroke—Adult (3–4 mo) *Gfap-cre*^{ERT2}/*Zeb2*$^{fl/fl}$ (Zeb2cKO) and *Zeb2*$^{fl/fl}$ (control) mice of both sexes that were approximately 25 g were administered tamoxifen (Sigma) by intraperitoneal IP injection at 100 mg/kg (2.5 mg in 0.1 ml of a 9:1 canola oil: ethanol mixture). Tamoxifen was delivered daily for five days prior to injury. As previously described (Kim et al., 2014; Woo et al., 2016; Yang et al., 2019), mice were subjected to transient middle cerebral artery occlusion (MCAO). Mice were anesthetized with isoflurane and a 6–0 Teflon-coated monofilament surgical suture (5–6 mm coating length; 0.25 mm diameter; cat# 602556PK10; Doccol Corp.) was inserted into the exposed external carotid artery, advanced into the internal carotid artery, and wedged into the Circle of Willis to block the origin of middle cerebral artery until the cerebral blood flow (CBF) had sufficiently dropped. CBF was blocked for 30 min before reperfusion, which was confirmed at the time of filament withdrawal. The CBF was measured by Laser-Doppler flowmeter (Periflux System 5010; Perimed AB) before MCAO, during occlusion period, and 10 min after reperfusion. Mice exhibiting greater than 80% reduction of pre-ischemic baseline CBF (20% of pre-stroke baseline) during MCAO and greater than 80% of pre-stroke baseline at 10 min of reperfusion were included in the study.

Post-Stroke Neurological Assessment—Neurological deficits in motor and reflex skills were assessed on the basis of motor and sensory tests on post-stroke days 1 and 3. Neurological scores were graded using a scale of 0 to 14 (0 indicating no deficits and 14 indicating maximum deficits)(Li et al., 2000). The motor function was tested by: 1) raising the mouse by its tail to assess forelimb flexion, hindlimb flexion, and head movement (>10° with respect to the vertical axis within 30 sec; scored 0–3); 2) placing a mouse on the floor to determine inability to walk straight, circling, and falling down to the paretic side (scored 0–3); 3) abnormal movements to assess immobility and staring, tremor, and seizures, myoclonus or myodystony (scored 0–3). Sensory tests were determined by a placing test (scored 0–2) and a proprioceptive test (scored 0–3). All post-stroke neurological assessments were carried out by investigators blinded to the animal's genotype. Assessment scores between control and *Zeb2cKO* mice were analyzed on Prism software (Graphpad Software) using two-tailed t-tests.

Tissue Collection—Mice were sacrificed by a lethal injection of ketamine and xylazine (150 mg/kg and 15 mg/kg, respectively; Henry Schein). For qRT-PCR and western blots with SCI mice, unfixed spinal cord tissue was isolated and prepared for analysis. For immunofluorescence analysis of SCI mice, tissue was fixed by trans-cardial perfusion with saline and heparin that was followed by 4% paraformaldehyde in Sorenson's buffer. Isolated spinal cords were post-fixed overnight before being cryoprotected with 30% sucrose in PBS and 20 μm sections were prepared for analyses. For all stroke-related analyses, isolated brains were flash-frozen before being cut into serial 20 μm sections at 600 μm intervals.

qRT-PCR—For SCI mice, 10 mm tissue blocks centered on the lesion were collected and placed in 0.5 ml of RNAlater (ThermoFisher) before being frozen at −80°C. Samples were batch-processed after collection of all experiment time points. Frozen tissue was ground with a pestle in a microcentrifuge tube that was immersed in dry ice/ethanol. RNA was isolated using QIAshredder columns (Qiagen) and RNAeasy mini kits (Qiagen) according to the manufacturer's instructions. RNA was quantified using a Nanodrop microvolume spectrophotometer (ThermoFisher) and cDNA was generated with the Superscript III First-Strand Synthesis kit (ThermoFisher). Real-time (RT) PCR amplification was performed with a QuantStudio Flex6 Real-Time PCR system (ThermoFisher). RT-PCR reactions to measure *Zeb1* expression levels used SYBR green PCR master mix (ThermoFisher) with *Zeb1* forward (5'-ACAAGACACCGCCGTCATTT-3') and reverse primers (5'-GCAGGTGAGCAACTGGGAAA-3'). RT-PCR reactions to measure *Zeb2* and *Zeb2os* expression levels used Taqman universal master mix and TaqMan assays (Mm00497193_m1 and Mm01269795_m1, respectively). All expression levels were normalized to *Gapdh* levels (using TaqMan assay Mm99999915_g1). All quantitative PCR data were analyzed on Prism software (Graphpad Software) by a 2-way ANOVA (a=0.05) followed by a Bonferroni's multiple comparisons test (α=0.05).

Western Blots—Protein samples were isolated from freshly dissected 10 mm spinal cord sections centered on the lesion that were mechanically homogenized. Total protein samples were generated with RIPA buffer containing protease inhibitors. Nuclear and cytoplasmic samples were generated using the NE-PER Nuclear and Cytoplasmic Extraction kit (ThermoFisher) and following the manufacturer's instructions. Protein concentrations were determined by DC assay (BioRad), as per the manufacturer's instructions. For western blotting, all protein samples were heat-denatured (95 °C, 5 min) prior to loading either 30 mg of nuclear protein, 50 μg of cytoplasmic, or 50 μg of total lysates per lane. Proteins were resolved by electrophoresis with pre-cast 8% acrylamide gels (BioRad) and then transferred to nitrocellulose membranes that were subsequently treated with Odyssey blocking buffer (LiCor). To visualize proteins, the nitrocellulose membranes were incubated with primary antibodies overnight at 4°C before being incubated with appropriate IRDye 680 or 800 secondary antibodies (1:10,000 dilution; LiCor) for 120 min at room temperature. Primary antibodies used were ZEB2 (1:1000, rabbit, Tarabykin laboratory), GFAP (1:1000, rabbit, Dako/Agilent), and p-actin (1:5000, mouse, Sigma). Membranes were imaged and band intensities were quantified using an Odyssey Imaging System (LiCor). Protein band intensities were normalized p-actin and analyzed on Prism software (Graphpad Software) using two-tailed t-tests.

Immunofluorescence—For SCI mice, horizontal longitudinal spinal cord tissue sections were blocked in phosphate buffer (PB) containing 5% Chemiblock, 0.5% Triton X-100, and 0.05% sodium azide for 30 minutes at room temperature. For mice with a stroke, tissue sections were fixed with 4% paraformaldehyde in phosphate buffer for 20 minutes at room temperature before being blocked in PB with 1 % BSA and 0.05% sodium azide for 60 minutes at room temperature. All tissue sections were incubated overnight at room temperature with primary antibodies in PB and 0.05% sodium azide (for SCI, PB also contained 5% Chemiblock, 0.1% Triton X-100, whereas PB for sections from mice with a

stroke also contained 0.5% BSA). Sections were then incubated with appropriate Alexa Fluor (ThermoFisher) secondary antibodies (1:1000 dilution) in PB for 2 hours at room temperature. Sections were mounted with ProLong Gold Antifade Reagent containing DAPI (ThermoFisher). The following primary antibodies and dilutions were used: CD11b (1:500, rat, Abcam), CD31 (1:5000, goat, R&D Systems), CD31 (1:200, rat, BD Biosciences), GFAP (1:500, goat, Santa Cruz Biotech), GFAP (1:1000, rabbit, Dako/Agilent), OLIG2 (1:500, mouse, Santa Cruz Biotech), NEUN (1:500, mouse, Millipore), ZEB2 (1:1000, rabbit, Tarabykin laboratory), ZEB1 (1:500, goat, Santa Cruz Biotech), β-ACTIN (1:5000, mouse, Sigma), and β-ACTIN (1:5000, rabbit, Sigma).

In Situ Hybridization—For *in situ* hybridization assays in the absence of immunofluorescence, assays were performed with RNAScope fluorescent multiplex detection reagents (ACDBio) and HybEZ hybridization system (ACDBio) according to the manufacturer's instructions. For co-labeling of tissue by *in situ* hybridization and immunofluorescence, tissue sections were post-fixed in paraformaldehyde in Sorenson's buffer at 4 °C for 30 minutes, then washed twice with PB before being submerged and boiled in Target Retrieval Buffer (ACDBio) at 98–99 °C for 5 minutes. Following antigen retrieval, sections were washed twice with distilled water and then dehydrated in 100% EtOH for 5 minutes. Sections were air-dried before a hydrophobic barrier was created with an ImmEdge pen (Vector Laboratories). Sections were then covered with RNAScope protease III solution (ACDBio) and incubated at 40 °C with a HybEZ hybridization system (ACDBio), after which sections were washed and then incubated with a *Zeb2os* C1 probe (ACDBio). Sections were subsequently treated according to the RNAScope fluorescent multiplex detection protocol (ACDBio). After the last wash, sections were blocked with 1% BSA and 0.1% Triton X-100 and then incubated overnight with primary GFAP antibody (Dako, 1:500 dilution). Sections were visualized with Alexa Fluor secondary antibodies (ThermoFisher, 1:000 dilution) and cover-slipped using Prolong Gold Antifade Reagent containing DAPI (ThermoFisher).

IgG Immunohistochemistry—Brain sections from mice with stroke were fixed with 4% paraformaldehyde for 15 minutes at room temperature, then treated with 3% H_2O_2 for 30 min to block endogenous peroxidase activity. Sections were washed and then incubated with a blocking solution containing 1% BSA and 10% normal goat serum for 1 hour at room temperature. Sections were then incubated overnight at 4 °C with anti-mouse IgG antibody (1:1000 dilution, Vector Laboratories) before being washed with PBS and then incubated with avidin/biotinylated peroxidase (ABC kit, Vector Laboratories) for 1 hour at room temperature. Antibody labeling was visualized using the diaminobenzidine (DAB) substrate (Sigma). For each mouse, IgG positive areas and hemispheric intensity ratios were measured with 3 sections spaced 600 pm throughout the lesion using Image J software (NIH) and analyzed with Prism software (Graphpad Software) using two-tailed t-tests. Analyses of IgG positive areas and hemispheric intensity ratios were carried out blinded to the animal's genotype.

Dextran Fluorescence—For mice with a stroke at 3 days post-injury, 25 mg/kg fluorescein isothiocyanate (FITC) conjugated 70 kDa Dextran (Sigma) was retro-orbitally

injected six hours prior to animal sacrifice and trans-cardial perfusion with PBS. Following perfusion, brains were flash-frozen and 20 pm sections were prepared with a cryostat. Sections were fixed with 4% paraformaldehyde in phosphate buffer and cover-slipped. For each mouse, Dextran fluorescence areas and intensities were measured in 3 sections spaced 600 pm throughout the lesion using Image J software (NIH) and analyzed with Prism software (Graphpad Software) using two-tailed t-tests. Analyses of dextran fluorescence areas and intensities were carried out blinded to the animal's genotype.

SCI Lesion Volume Analysis—A 12.7 mm (0.5 inch) block of the spinal cord tissue centered on the injury epicenter was used to generate five sets of 20 μm-thick longitudinal, horizontal sections. For each mouse, GFAP and CD11 b expression was visualized by immunofluorescence in a set of serial sections that spanned the entire dorsal-ventral axis (consisting of 20–25 sections per mouse). Entire sections were imaged at 10X on a Zeiss Axiolmager M2 epifluorescence microscope and composite images for sections were tiled using the Virtual Tissue Section Manager as part of Stereo Investigator (MBF Bioscience). Lesions volumes determined using Neurolucida (MBF Bioscience) with lesion boundaries defined by the margins of CD11b+, GFAP− staining. Lesion tracing and reconstructions were carried out blinded to the animal's genotype. Lesion volumes were analyzed by a two-tailed t-test with Prism software (Graphpad Software).

Infarct Volume and Brain Swelling in Mice with a Stroke—Three days after stroke, 20 μm-thick sections were serially collected at 600 pm intervals across a ~7.3 mm region spanning the rostro-caudal axis (approximately +3.1 mm and −4.2 mm from bregma). A total of 13 sections were used for infarct size and swelling measurements, which were performed with Axiovision software (Zeiss). As previously described (Kim et al., 2014; Yang et al., 2019), brain sections were examined by phase contrast microscopy and infarct territories were traced within each section to calculate the infarct area. The percent hemispheric swelling was calculated by dividing the difference between ipsilateral and contralateral hemispheric volume by contralateral hemispheric volume and multiplying by 100. Infarct volume and brain swelling analyses were carried out blinded to the animal's genotype. Infarct volumes and percent swelling were each analyzed by two-tailed t-tests using with Prism software (Graphpad Software).

QUANTIFICATION AND STATISTICAL ANALYSIS

Sample sizes were based on previous experience and statistical methods were not used to predetermine sample size. Data are presented as the mean ± standard error of the mean (SEM). Sample sizes (n) of either animals or the number of experimental repeats, as well as statistical methods and results are provided in the corresponding figure legends. Comparisons between two groups were made using two-tailed unpaired Student's t tests, otherwise one way- or two-way ANOVA with repeated-measures applied when appropriate were used. Bonferroni post-hoc correction tests were employed following ANOVA comparisons. Differences were considered statistically significant when p values were below 0.05. All data were analyzed using Prism software (GraphPad Software) and post-hoc power calculations were performed with G*Power (Faul et al., 2009).

Supplementary Material

Refer to Web version on PubMed Central for supplementary material.

Acknowledgements

Funding for this work was provided by the NYS DOH SCIRB grant C33266GG (JWC), the Burke Neurological Institute (JWC), and DFG grant TA303/8-1 (VST)

References

Abba ML, Patil N, Leupold JH, and Allgayer H (2016). MicroRNA Regulation of Epithelial to Mesenchymal Transition. J Clin Med 5.

Anderson MA, Burda JE, Ren Y, Ao Y, O'Shea TM, Kawaguchi R, Coppola G, Khakh BS, Deming TJ, and Sofroniew MV (2016). Astrocyte scar formation aids central nervous system axon regeneration. Nature 532, 195–200. [PubMed: 27027288]

Barnabe-Heider F, Goritz C, Sabelstrom H, Takebayashi H, Pfrieger FW, Meletis K, and Frisen J (2010). Origin of new glial cells in intact and injured adult spinal cord. Cell Stem Cell 7, 470–482. [PubMed: 20887953]

Becerra-Calixto A, and Cardona-Gomez GP (2017). The Role of Astrocytes in Neuroprotection after Brain Stroke: Potential in Cell Therapy. Front Mol Neurosci 10, 88. [PubMed: 28420961]

Beltran M, Puig I, Pena C, Garcia JM, Alvarez AB, Pena R, Bonilla F, and de Herreros AG (2008). A natural antisense transcript regulates Zeb2/Sip1 gene expression during Snail1-induced epithelial-mesenchymal transition. Genes Dev 22, 756–769. [PubMed: 18347095]

Benner EJ, Luciano D, Jo R, Abdi K, Paez-Gonzalez P, Sheng H, Warner DS, Liu C, Eroglu C, and Kuo CT (2013). Protective astrogenesis from the SVZ niche after injury is controlled by Notch modulator Thbs4. Nature 497, 369–373. [PubMed: 23615612]

Bhalala OG, Pan L, Sahni V, McGuire TL, Gruner K, Tourtellotte WG, and Kessler JA (2012). microRNA-21 regulates astrocytic response following spinal cord injury. J Neurosci 32, 17935–17947. [PubMed: 23238710]

Brambilla R, Bracchi-Ricard V, Hu WH, Frydel B, Bramwell A, Karmally S, Green EJ, and Bethea JR (2005). Inhibition of astroglial nuclear factor kappaB reduces inflammation and improves functional recovery after spinal cord injury. J Exp Med 202, 145–156. [PubMed: 15998793]

Burda JE, and Sofroniew MV (2014). Reactive gliosis and the multicellular response to CNS damage and disease. Neuron 81, 229–248. [PubMed: 24462092]

Bush TG, Puvanachandra N, Horner CH, Polito A, Ostenfeld T, Svendsen CN, Mucke L, Johnson MH, and Sofroniew MV (1999). Leukocyte infiltration, neuronal degeneration, and neurite outgrowth after ablation of scar-forming, reactive astrocytes in adult transgenic mice. Neuron 23, 297–308. [PubMed: 10399936]

Carlen M, Meletis K, Goritz C, Darsalia V, Evergren E, Tanigaki K, Amendola M, Barnabe-Heider F, Yeung MS, Naldini L, et al. (2009). Forebrain ependymal cells are Notch-dependent and generate neuroblasts and astrocytes after stroke. Nat Neurosci 12, 259–267. [PubMed: 19234458]

Chng Z, Teo A, Pedersen RA, and Vallier L (2010). SIP1 mediates cell-fate decisions between neuroectoderm and mesendoderm in human pluripotent stem cells. Cell Stem Cell 6, 59–70. [PubMed: 20074535]

Dang LT, and Tropepe V (2010). FGF dependent regulation of Zfhx1b gene expression promotes the formation of definitive neural stem cells in the mouse anterior neurectoderm. Neural Dev 5, 13. [PubMed: 20459606]

Dang LT, Wong L, and Tropepe V (2012). Zfhx1b induces a definitive neural stem cell fate in mouse embryonic stem cells. Stem Cells Dev 21, 2838–2851. [PubMed: 22594450]

Epifanova E, Babaev A, Newman AG, and Tarabykin V (2019). Role of Zeb2/Sip1 in neuronal development. Brain Res 1705, 24–31. [PubMed: 30266271]

Faiz M, Sachewsky N, Gascon S, Bang KW, Morshead CM, and Nagy A (2015). Adult Neural Stem Cells from the Subventricular Zone Give Rise to Reactive Astrocytes in the Cortex after Stroke. Cell Stem Cell 17, 624–634. [PubMed: 26456685]

Faul F, Erdfelder E, Buchner A, and Lang AG (2009). Statistical power analyses using G*Power 3.1: tests for correlation and regression analyses. Behav Res Methods 41, 1149–1160. [PubMed: 19897823]

Faulkner JR, Herrmann JE, Woo MJ, Tansey KE, Doan NB, and Sofroniew MV (2004). Reactive astrocytes protect tissue and preserve function after spinal cord injury. J Neurosci 24, 2143–2155. [PubMed: 14999065]

Fouani L, Huang MLH, Cole L, Jansson PJ, Kovacevic Z, and Richardson DR (2020). During mitosis ZEB1 switches from being a chromatin-bound epithelial gene repressor, to become a microtubule-associated protein. Biochim Biophys Acta Mol Cell Res, 118673. [PubMed: 32057919]

Ganat YM, Silbereis J, Cave C, Ngu H, Anderson GM, Ohkubo Y, Ment LR, and Vaccarino FM (2006). Early postnatal astroglial cells produce multilineage precursors and neural stem cells in vivo. J Neurosci 26, 8609–8621. [PubMed: 16914687]

Gleichman AJ, and Carmichael ST (2014). Astrocytic therapies for neuronal repair in stroke. Neurosci Lett 565, 47–52. [PubMed: 24184876]

Haensel D, and Dai X (2018). Epithelial-to-mesenchymal transition in cutaneous wound healing: Where we are and where we are heading. Dev Dyn 247, 473–480. [PubMed: 28795450]

Hamers FP, Koopmans GC, and Joosten EA (2006). CatWalk-assisted gait analysis in the assessment of spinal cord injury. J Neurotrauma 23, 537–548. [PubMed: 16629635]

Hamers FP, Lankhorst AJ, van Laar TJ, Veldhuis WB, and Gispen WH (2001). Automated quantitative gait analysis during overground locomotion in the rat: its application to spinal cord contusion and transection injuries. J Neurotrauma 18, 187–201. [PubMed: 11229711]

He L, Yu K, Lu F, Wang J, Wu LN, Zhao C, Li Q, Zhou X, Liu H, Mu D, et al. (2018). Transcriptional Regulator ZEB2 Is Essential for Bergmann Glia Development. J Neurosci 38, 1575–1587. [PubMed: 29326173]

Hegarty SV, Sullivan AM, and O'Keeffe GW (2015). Zeb2: A multifunctional regulator of nervous system development. Prog Neurobiol 132, 81–95. [PubMed: 26193487]

Herrmann JE, Imura T, Song B, Qi J, Ao Y, Nguyen TK, Korsak RA, Takeda K, Akira S, and Sofroniew MV (2008). STAT3 is a critical regulator of astrogliosis and scar formation after spinal cord injury. J Neurosci 28, 7231–7243. [PubMed: 18614693]

Higashi Y, Maruhashi M, Nelles L, Van de Putte T, Verschueren K, Miyoshi T, Yoshimoto A, Kondoh H, and Huylebroeck D (2002). Generation of the floxed allele of the SIP1 (Smad-interacting protein 1) gene for Cre-mediated conditional knockout in the mouse. Genesis 32, 82–84. [PubMed: 11857784]

Hill CS (2009). Nucleocytoplasmic shuttling of Smad proteins. Cell Res 19, 36–46. [PubMed: 19114992]

Hsu JY, Bourguignon LY, Adams CM, Peyrollier K, Zhang H, Fandel T, Cun CL, Werb Z, and Noble-Haeusslein LJ (2008). Matrix metalloproteinase-9 facilitates glial scar formation in the injured spinal cord. J Neurosci 28, 13467–13477. [PubMed: 19074020]

Jere SW, Abrahamse H, and Houreld NN (2017). The JAK/STAT signaling pathway and photobiomodulation in chronic wound healing. Cytokine Growth Factor Rev 38, 73–79. [PubMed: 29032938]

Johansson CB, Momma S, Clarke DL, Risling M, Lendahl U, and Frisen J (1999). Identification of a neural stem cell in the adult mammalian central nervous system. Cell 96, 25–34. [PubMed: 9989494]

Kim E, Tolhurst AT, and Cho S (2014). Deregulation of inflammatory response in the diabetic condition is associated with increased ischemic brain injury. J Neuroinflammation 11, 83. [PubMed: 24886035]

Lamouille S, Xu J, and Derynck R (2014). Molecular mechanisms of epithelial-mesenchymal transition. Nat Rev Mol Cell Biol 15, 178–196. [PubMed: 24556840]

Li N, Babaei-Jadidi R, Lorenzi F, Spencer-Dene B, Clarke P, Domingo E, Tulchinsky E, Vries RGJ, Kerr D, Pan Y, et al. (2019). An FBXW7-ZEB2 axis links EMT and tumour microenvironment to

promote colorectal cancer stem cells and chemoresistance. Oncogenesis 8, 13. [PubMed: 30783098]

Li Y, Chopp M, Chen J, Wang L, Gautam SC, Xu YX, and Zhang Z (2000). Intrastriatal transplantation of bone marrow nonhematopoietic cells improves functional recovery after stroke in adult mice. J Cereb Blood Flow Metab 20, 1311–1319. [PubMed: 10994853]

Li ZW, Tang RH, Zhang JP, Tang ZP, Qu WS, Zhu WH, Li JJ, Xie MJ, Tian DS, and Wang W (2011). Inhibiting epidermal growth factor receptor attenuates reactive astrogliosis and improves functional outcome after spinal cord injury in rats. Neurochem Int 58, 812–819. [PubMed: 21402118]

Liddelow SA, and Barres BA (2017). Reactive Astrocytes: Production, Function, and Therapeutic Potential. Immunity 46, 957–967. [PubMed: 28636962]

Liu Z, and Chopp M (2016). Astrocytes, therapeutic targets for neuroprotection and neurorestoration in ischemic stroke. Prog Neurobiol 144, 103–120. [PubMed: 26455456]

Long J, Zuo D, and Park M (2005). Pc2-mediated sumoylation of Smad-interacting protein 1 attenuates transcriptional repression of E-cadherin. J Biol Chem 280, 35477–35489. [PubMed: 16061479]

Mahabir R, Tanino M, Elmansuri A, Wang L, Kimura T, Itoh T, Ohba Y, Nishihara H, Shirato H, Tsuda M, et al. (2014). Sustained elevation of Snail promotes glial-mesenchymal transition after irradiation in malignant glioma. Neuro Oncol 16, 671–685. [PubMed: 24357458]

Mamber C, Kozareva DA, Kamphuis W, and Hol EM (2013). Shades of gray: The delineation of marker expression within the adult rodent subventricular zone. Prog Neurobiol 111, 1–16. [PubMed: 23994259]

McKinsey GL, Lindtner S, Trzcinski B, Visel A, Pennacchio LA, Huylebroeck D, Higashi Y, and Rubenstein JL (2013). Dlx1&2-dependent expression of Zfhx1b (Sip1, Zeb2) regulates the fate switch between cortical and striatal interneurons. Neuron 77, 83–98. [PubMed: 23312518]

Meletis K, Barnabe-Heider F, Carlen M, Evergren E, Tomilin N, Shupliakov O, and Frisen J (2008). Spinal cord injury reveals multilineage differentiation of ependymal cells. PLoS Biol 6, e182. [PubMed: 18651793]

Miquelajauregui A, Van de Putte T, Polyakov A, Nityanandam A, Boppana S, Seuntjens E, Karabinos A, Higashi Y, Huylebroeck D, and Tarabykin V (2007). Smad-interacting protein-1 (Zfhx1b) acts upstream of Wnt signaling in the mouse hippocampus and controls its formation. Proc Natl Acad Sci U S A 104, 12919–12924. [PubMed: 17644613]

Nieto MA, Huang RY, Jackson RA, and Thiery JP (2016). Emt: 2016. Cell 166, 21–45. [PubMed: 27368099]

Nitta KR, Tanegashima K, Takahashi S, and Asashima M (2004). XSIP1 is essential for early neural gene expression and neural differentiation by suppression of BMP signaling. Dev Biol 275, 258–267. [PubMed: 15464588]

Okada S, Nakamura M, Katoh H, Miyao T, Shimazaki T, Ishii K, Yamane J, Yoshimura A, Iwamoto Y, Toyama Y, et al. (2006). Conditional ablation of Stat3 or Socs3 discloses a dual role for reactive astrocytes after spinal cord injury. Nat Med 12, 829–834. [PubMed: 16783372]

Pekny M, and Pekna M (2014). Astrocyte reactivity and reactive astrogliosis: costs and benefits. Physiol Rev 94, 1077–1098. [PubMed: 25287860]

Ren Y, Ao Y, O'Shea TM, Burda JE, Bernstein AM, Brumm AJ, Muthusamy N, Ghashghaei HT, Carmichael ST, Cheng L, et al. (2017). Ependymal cell contribution to scar formation after spinal cord injury is minimal, local and dependent on direct ependymal injury. Sci Rep 7, 41122. [PubMed: 28117356]

Rogers CD, Saxena A, and Bronner ME (2013). Sip1 mediates an E-cadherin-to-N-cadherin switch during cranial neural crest EMT. J Cell Biol 203, 835–847. [PubMed: 24297751]

Sabelstrom H, Stenudd M, Reu P, Dias DO, Elfineh M, Zdunek S, Damberg P, Goritz C, and Frisen J (2013). Resident neural stem cells restrict tissue damage and neuronal loss after spinal cord injury in mice. Science 342, 637–640. [PubMed: 24179227]

Sahni V, Mukhopadhyay A, Tysseling V, Hebert A, Birch D, McGuire TL, Stupp SI, and Kessler JA (2010). BMPR1a and BMPR1b signaling exert opposing effects on gliosis after spinal cord injury. J Neurosci 30, 1839–1855. [PubMed: 20130193]

Seuntjens E, Nityanandam A, Miquelajauregui A, Debruyn J, Stryjewska A, Goebbels S, Nave KA, Huylebroeck D, and Tarabykin V (2009). Sip1 regulates sequential fate decisions by feedback signaling from postmitotic neurons to progenitors. Nat Neurosci 12, 1373–1380. [PubMed: 19838179]

Sofroniew MV (2009). Molecular dissection of reactive astrogliosis and glial scar formation. Trends Neurosci 32, 638–647. [PubMed: 19782411]

Sofroniew MV (2014). Astrogliosis. Cold Spring Harb Perspect Biol 7, a020420. [PubMed: 25380660]

Stone RC, Pastar I, Ojeh N, Chen V, Liu S, Garzon KI, and Tomic-Canic M (2016). Epithelial-mesenchymal transition in tissue repair and fibrosis. Cell Tissue Res 365, 495–506. [PubMed: 27461257]

Stroncek JD, and Reichert WM (2008). Overview of Wound Healing in Different Tissue Types. In Indwelling Neural Implants: Strategies for Contending with the In Vivo Environment, Reichert WM, ed. (Boca Raton (FL)).

Subramanian A, Tamayo P, Mootha VK, Mukherjee S, Ebert BL, Gillette MA, Paulovich A, Pomeroy SL, Golub TR, Lander ES, et al. (2005). Gene set enrichment analysis: a knowledge-based approach for interpreting genome-wide expression profiles. Proc Natl Acad Sci U S A 102, 15545–15550. [PubMed: 16199517]

Takagi T, Moribe H, Kondoh H, and Higashi Y (1998). DeltaEF1, a zinc finger and homeodomain transcription factor, is required for skeleton patterning in multiple lineages. Development 125, 21–31. [PubMed: 9389660]

Van de Putte T, Maruhashi M, Francis A, Nelles L, Kondoh H, Huylebroeck D, and Higashi Y (2003). Mice lacking ZFHX1B, the gene that codes for Smad-interacting protein-1, reveal a role for multiple neural crest cell defects in the etiology of Hirschsprung disease-mental retardation syndrome. Am J Hum Genet 72, 465–470. [PubMed: 12522767]

van Grunsven LA, Taelman V, Michiels C, Verstappen G, Souopgui J, Nichane M, Moens E, Opdecamp K, Vanhomwegen J, Kricha S, et al. (2007). XSip1 neuralizing activity involves the co-repressor CtBP and occurs through BMP dependent and independent mechanisms. Dev Biol 306, 34–49. [PubMed: 17442301]

Vandewalle C, Van Roy F, and Berx G (2009). The role of the ZEB family of transcription factors in development and disease. Cell Mol Life Sci 66, 773–787. [PubMed: 19011757]

Wanner IB, Anderson MA, Song B, Levine J, Fernandez A, Gray-Thompson Z, Ao Y, and Sofroniew MV (2013). Glial scar borders are formed by newly proliferated, elongated astrocytes that interact to corral inflammatory and fibrotic cells via STAT3-dependent mechanisms after spinal cord injury. J Neurosci 33, 12870–12886. [PubMed: 23904622]

Weng Q, Chen Y, Wang H, Xu X, Yang B, He Q, Shou W, Chen Y, Higashi Y, van den Berghe V, et al. (2012). Dual-mode modulation of Smad signaling by Smad-interacting protein Sip1 is required for myelination in the central nervous system. Neuron 73, 713–728. [PubMed: 22365546]

White RE, Rao M, Gensel JC, McTigue DM, Kaspar BK, and Jakeman LB (2011). Transforming growth factor alpha transforms astrocytes to a growth-supportive phenotype after spinal cord injury. J Neurosci 31, 15173–15187. [PubMed: 22016551]

Woo MS, Yang J, Beltran C, and Cho S (2016). Cell Surface CD36 Protein in Monocyte/Macrophage Contributes to Phagocytosis during the Resolution Phase of Ischemic Stroke in Mice. J Biol Chem 291, 23654–23661. [PubMed: 27646002]

Yan C, Grimm WA, Garner WL, Qin L, Travis T, Tan N, and Han YP (2010). Epithelial to mesenchymal transition in human skin wound healing is induced by tumor necrosis factor-alpha through bone morphogenic protein-2. Am J Pathol 176, 2247–2258. [PubMed: 20304956]

Yang J, Balkaya M, Beltran C, Heo JH, and Cho S (2019). Remote Postischemic Conditioning Promotes Stroke Recovery by Shifting Circulating Monocytes to CCR2(+) Proinflammatory Subset. J Neurosci 39, 7778–7789. [PubMed: 31427395]

Zeisberg M, and Neilson EG (2009). Biomarkers for epithelial-mesenchymal transitions. J Clin Invest 119, 1429–1437. [PubMed: 19487819]

Zhao X, Wang D, Ding Y, Zhou J, Liu G, and Ji Z (2019). lncRNA ZEB1-AS1 promotes migration and metastasis of bladder cancer cells by post-transcriptional activation of ZEB1. Int J Mol Med 44, 196–206. [PubMed: 31115480]

Zheng H, and Kang Y (2014). Multilayer control of the EMT master regulators. Oncogene 33, 1755–1763. [PubMed: 23604123]

Highlights

- *Zeb2* promotes astrogliosis and preservation of neurological function after injury
- Naïve astrocytes have *Zeb2* mRNA, but protein expression is induced only after injury
- Stroke and SCI also modify expression of several lncRNAs, including *Zeb2os*
- Role of *Zeb2* and gene expression changes suggest astrogliosis is an EMT-like process

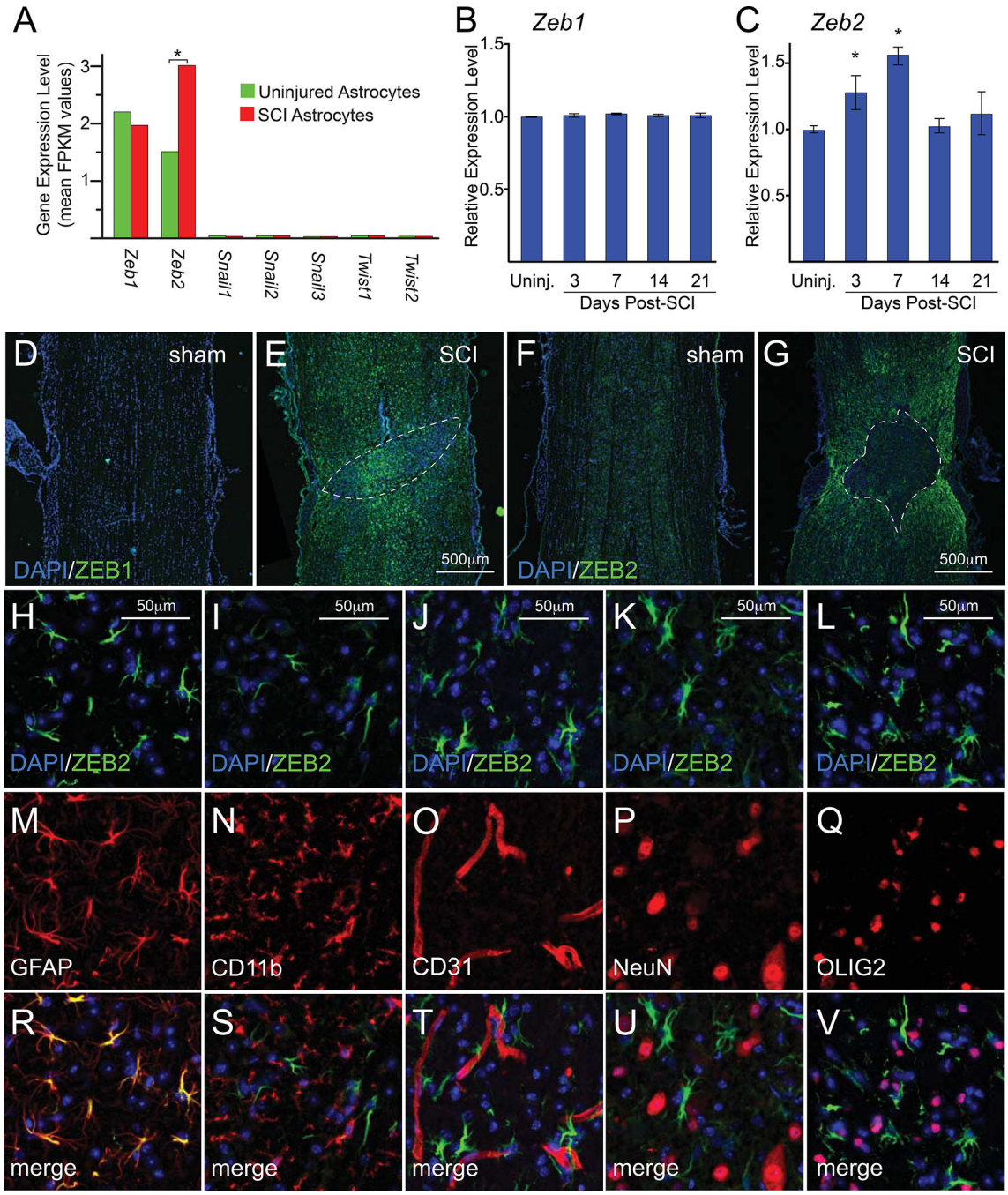

Figure 1.

Expression of *Zeb1/2* following SCI. **A**, expression levels from RNA-seq data (Anderson et al., 2016) for canonical EMT transcription factor gene families *(Snail, Twist,* and *Zeb)* in astrocytes from uninjured mice and reactive astrocytes 14 days after SCI. Asterisks indicate significant changes indicated in expression levels, as indicated by the database (Anderson et al., 2016). **B** and **C**, time course qRT-PCR analysis of whole spinal cord tissue from either uninjured mice or those with SCI for *Zeb1* and *Zeb2,* respectively. Asterisks indicate significant changes relative to uninjured mice (for both B and C: one-way ANOVA, n=3 for

each time point and 3 technical repeats for each time point; and power=0.99 and 0.82 for B and C, respectively; asterisks indicate $p<0.04$ for C). **D**-**G**, immunofluorescence of spinal cord ZEB1 and ZEB2 expression in sham and SCI mice 14 days after injury. Lesions are outlined by white dashed lines. **H**-**V**, immunofluorescence analysis in the spinal cord 14 days after injury at ~1500μm from the lesion shows ZEB2 was expressed in nearly all astrocytes (GFAP), but absent from oligodendrocytes (OLIG2), neurons (NeuN), microglia/macrophages (CD11b), and endothelial cells (CD31). See also Supplemental Figures S1–S3.

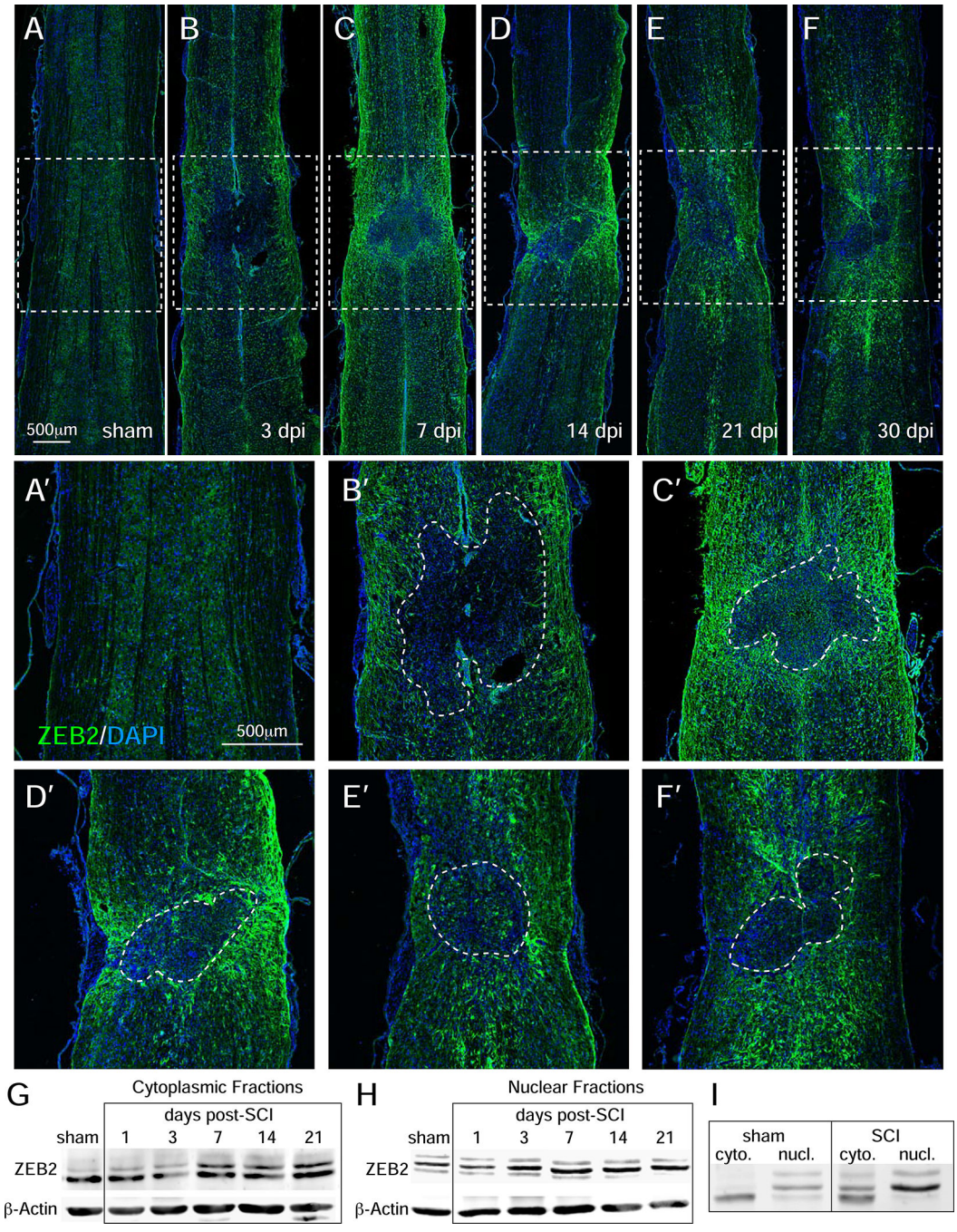

Figure 2.

Immunofluorescence time-course analysis of SCI-induced ZEB2 expression. **A**-**F**, immunofluorescence shows that ZEB2 expression around the lesion after SCI peaks between 7 and 14 days after SCI. Lesions are outlined by white dashed lines. **G** and **H**, western blot time course analysis of whole spinal cord tissue show multiple ZEB2 isoforms in cytoplasmic and nuclear fractions, respectively. **I**, western blots showing the relative sizes of ZEB2 isoforms in the cytoplasmic and nuclear fractions.

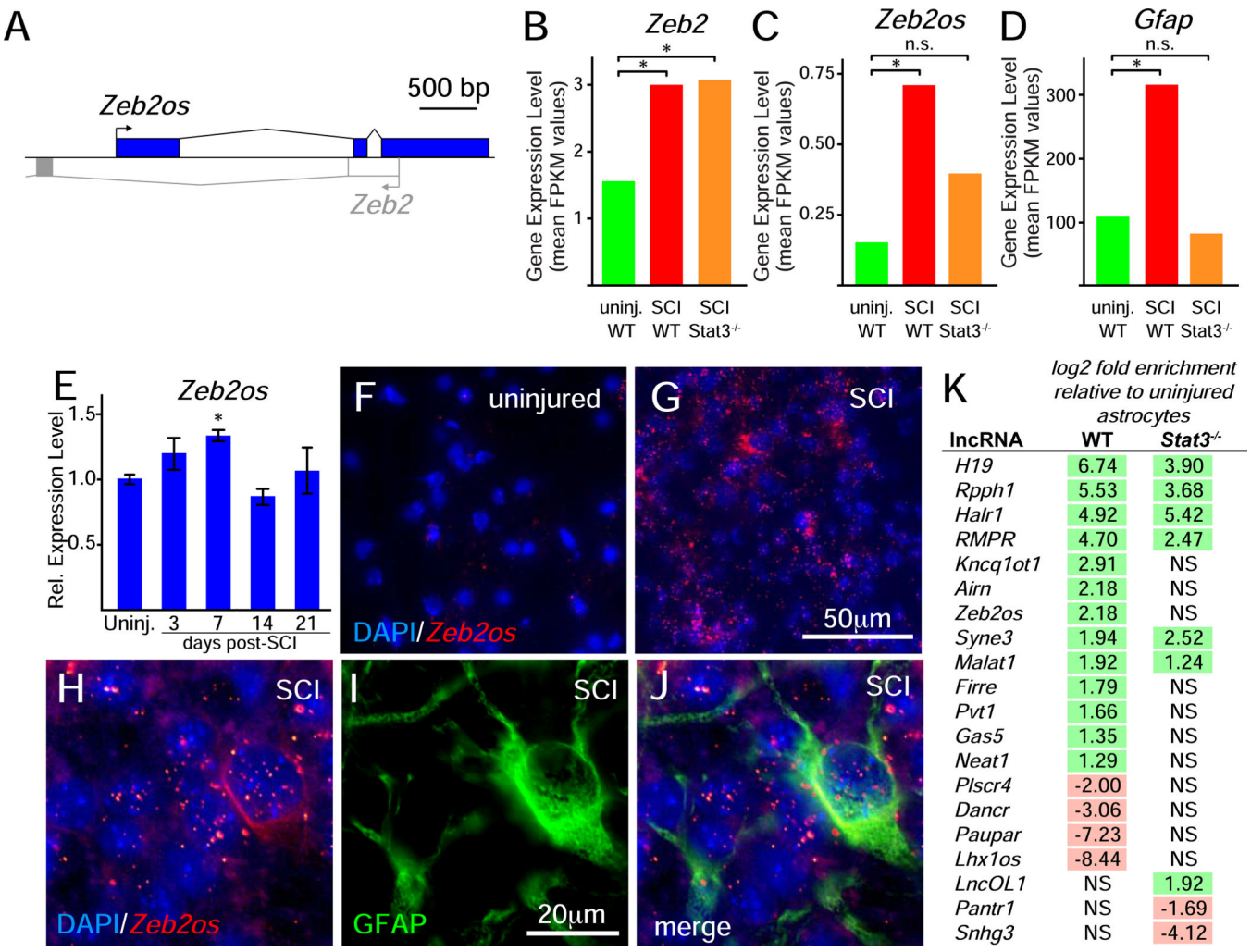

lncRNA	WT	*Stat3*$^{-/-}$
H19	6.74	3.90
Rpph1	5.53	3.68
Halr1	4.92	5.42
RMPR	4.70	2.47
Kncq1ot1	2.91	NS
Airn	2.18	NS
Zeb2os	2.18	NS
Syne3	1.94	2.52
Malat1	1.92	1.24
Firre	1.79	NS
Pvt1	1.66	NS
Gas5	1.35	NS
Neat1	1.29	NS
Plscr4	-2.00	NS
Dancr	-3.06	NS
Paupar	-7.23	NS
Lhx1os	-8.44	NS
LncOL1	NS	1.92
Pantr1	NS	-1.69
Snhg3	NS	-4.12

Figure 3.

Injury-induced *Zeb2os* expression following SCI. **A**, schematic of the overlapping genomic structure of mouse *Zeb2os* and *Zeb2.* **B-D**, RNA-seq data (Anderson et al., 2016) for *Zeb2, Zeb2os,* and *Gfap* expression in astrocytes from uninjured mice and reactive astrocytes 14 days after SCI in either wild-type (WT) or *Stat3*$^{-/-}$–. Asterisks indicate significant changes in expression levels relative to uninjured astrocytes, as indicated by the database (Anderson et al., 2016). **E**, qRT-PCR time course analysis of *Zeb2os* expression in whole spinal cord tissue following SCI. Asterisks indicate significant changes relative to uninjured mice (one-way ANOVA, asterisk indicates $p<0.01$; n=3 for each time point and 3 technical repeats for each time point, power=0.60). **F** and **G**, *in situ* hybridization assays showing *Zeb2os* expression levels in uninjured mice and SCI mice 7 days post-injury, respectively. **H-J**, *in situ* hybridization and immunofluorescence assays in gray matter tissue from SCI mice 7 days post-injury showing the upregulation of *Zeb2os* expression in and around GFAP-expressing astrocytes. In injured tissue, images were collected approximately 250 pm from the lesion border. **K**, RNA-seq data (Anderson et al., 2016) for IncRNAs with expression levels that significantly change following SCI in WT and/or *Stat3*$^{-/-}$ astrocytes 14 days following SCI. Significant changes are indicated in the log2-fold change and non-significant

changes are indicated by “NS,” as indicated in the database (Anderson et al., 2016). See also Supplemental Figure S4.

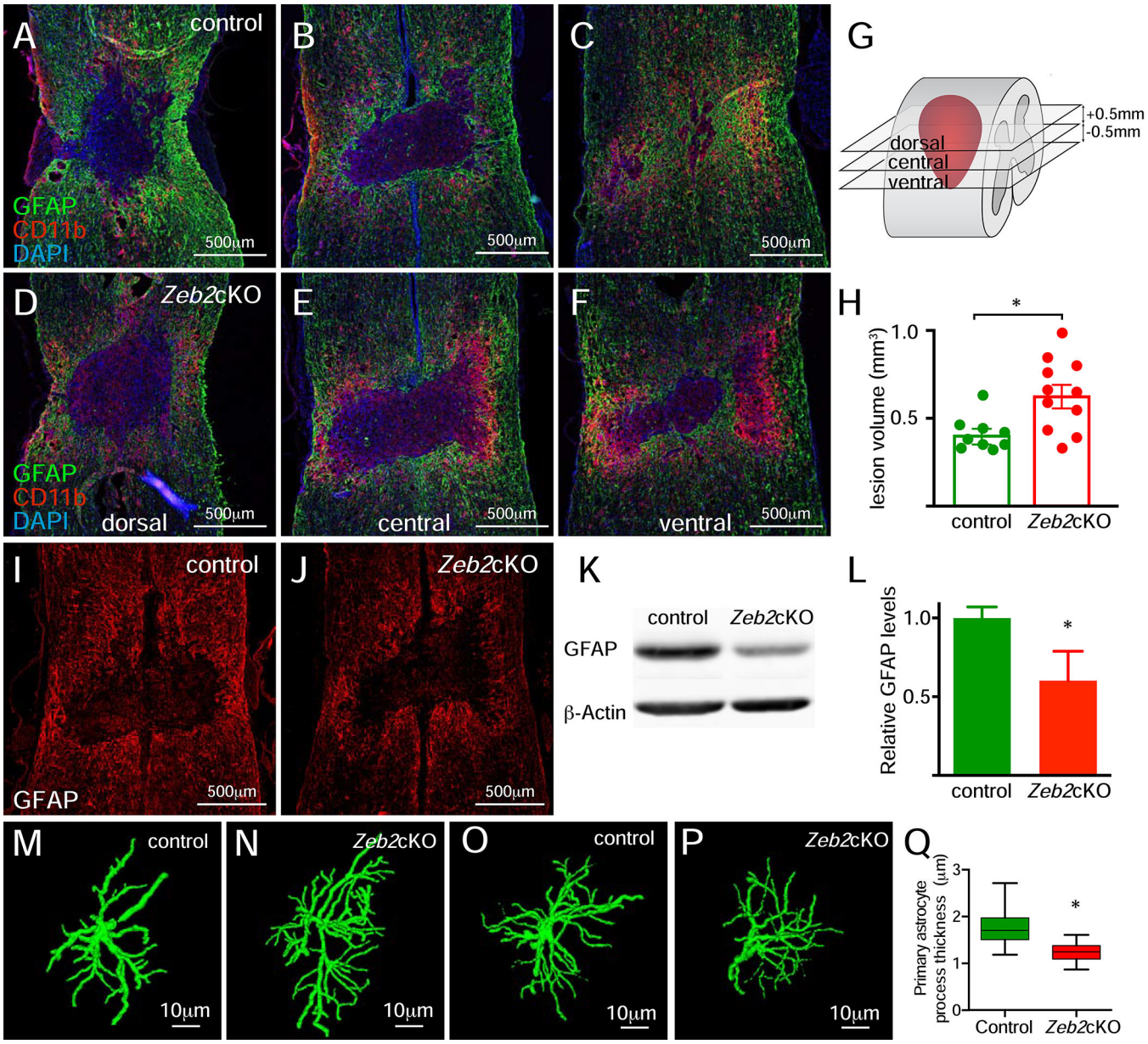

Figure 4.

Attenuated astrogliosis and increased lesion volumes after SCI in *Zeb2cKO* mice. **A-C** and **D-F**, immunofluorescence for GFAP (astrocytes) and microglia/macrophages (CD11b) expression in the spinal cord in control and *Zeb2*cKO mice, respectively, at 14 days post-SCI reveals larger lesion volumes in *Zeb2cKO* mice. **G**, relative positions in the spinal cord of sections shown in A-F, which are centered on the central canal. **H**, lesion volume measurements show that lesion volumes are increased in Zeb2*cKO* mice (unpaired Student t test, n=9 for control and n= 11 for Zeb2*cKO* mice, $p<0.01$, and power=0.92). **I** and **J**, immunofluorescence for GFAP expression in control and Zeb2*cKO* mice, respectively. **K**, western blot analysis of GFAP expression in whole spinal cord tissue from control and Zeb2*cKO* mice. **L**, quantification of western blot band intensities shows a significant

decrease in GFAP expression levels, relative to β-Actin (unpaired Student t test, n=3 for each genotype, $p<0.03$, power=0.73). **M**-**N** and **O**-**P**, show astrocyte reconstructions using GFAP expression in reactive astrocytes at 1mm and 3 mm, respectively, from the lesion for control and Zeb2*cKO* mice. **Q**, measurements of primary process thickness in reconstructed astrocytes at 1 mm from the lesion shows that astrocytes in Zeb2*cKO* mice have thinner processes than control mice (unpaired, nested Student t test, n=3 animals of each genotype with 42 and 55 measurements for control and *Zeb2*cKO, respectively, $p<0.01$).

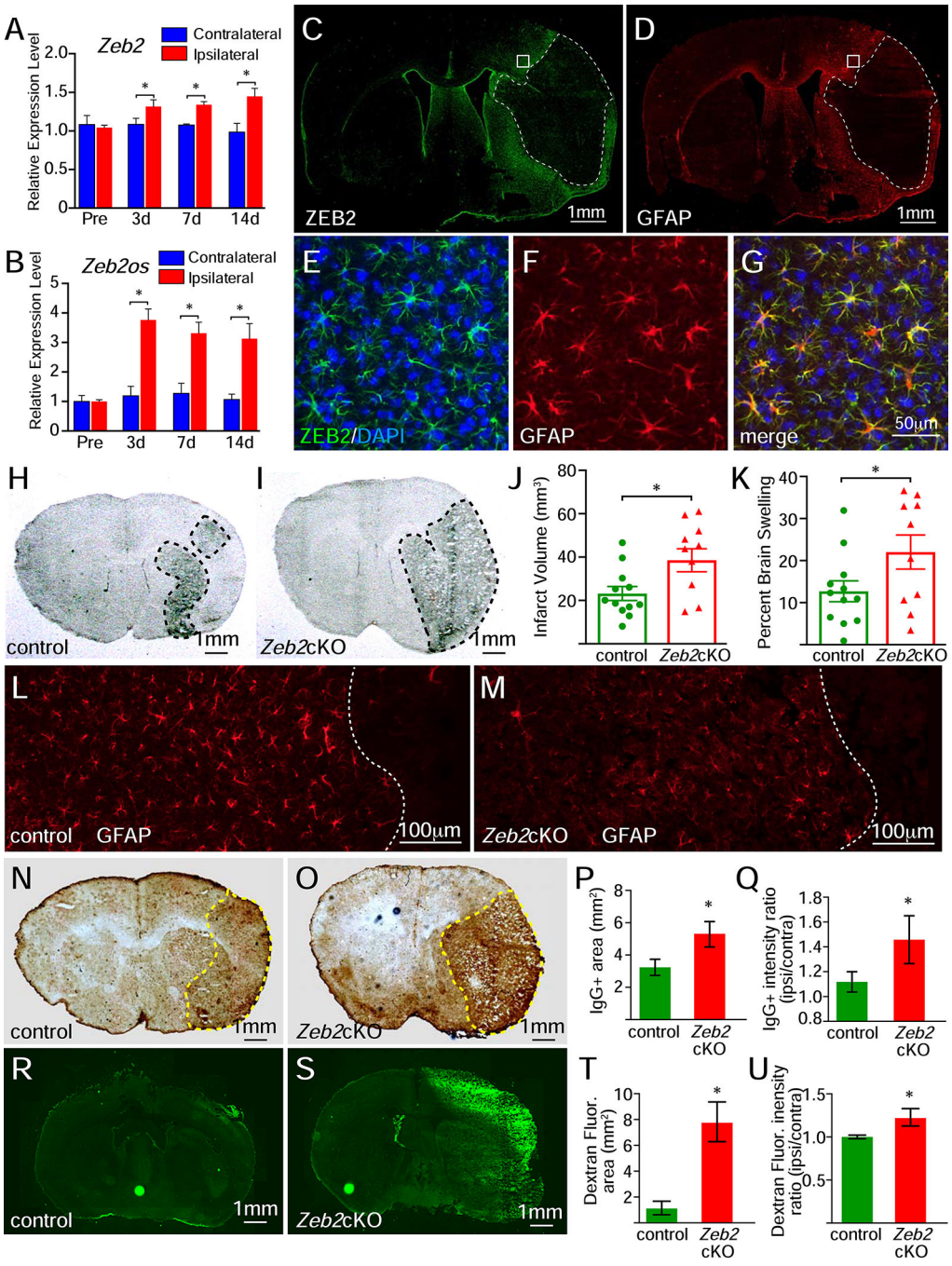

Figure 5.

Injury-induced ZEB2 expression and attenuation of astrogliosis in *Zeb2cKO* mice following ischemic stroke. **A** and **B**, the relative expression levels for *Zeb2* and *Zeb2os* significantly increased in the ipsilateral hemisphere, relative to the contralateral hemisphere, following ischemic stroke (two-way ANOVA, n=3 for both *Zeb2* and *Zeb2os,* asterisks indicate $p<0.01$, power=0.99 for A and B, respectively). **C-G**, immunofluorescence for ZEB2 and GFAP expression in the same section 3 days post-stroke shows a strong induction of ZEB2 expression in reactive astrocytes surrounding the infarct. Infarct regions in C and D are

outlined with dashed white lines and region shown in E-G are indicated by white boxes. **H** and **I**, coronal brain sections from control and *Zeb2cKO* mice, respectively, showing infarct regions at 3 days post-stroke. Infarct regions are outlined with black dashed lines. **J**, lesion volumes in 3-day post-stroke brains (unpaired Student t test, n=12 for control and n=10 for *Zeb2*cKO, $p<0.01$, power=0.78). **K**, brain swelling in 3-day post-stroke brains (unpaired Student t test, n=12 for control and n=10 for *Zeb2*cKO, $p<0.05$, power=0.47). **L** and **M**, immunofluorescence for GFAP expression control and Zeb2*cKO* mice, respectively. **N** and **O**, immunohistochemistry for IgG in brain sections control and Zeb2*cKO* mice with stroke, respectively. IgG+ territories are outlined by yellow dashed lines. **P**, area of IgG staining in 3-day post-stroke brains (unpaired Student t test, n=6 for each genotype, $p<0.05$, power=0.99). **Q**, interhemispheric ratio of IgG staining intensity in 3-day post-stroke brains (unpaired Student t test, n=6 for each genotype, $p<0.05$, power=0.99). **R** and **S**, Dextran fluorescence in brain sections from control and *Zeb2cKO* mice with stroke, respectively. **T**, area of Dextran fluorescence in 3-day post-stroke brains (unpaired Student t test, n=3 for each genotype, $p<0.01$, power=0.99). **U**, interhemispheric ratio of Dextran fluorescence intensity in 3-day post-stroke brains (unpaired Student t test, n=3 for each genotype, $p<0.05$, power=0.99).

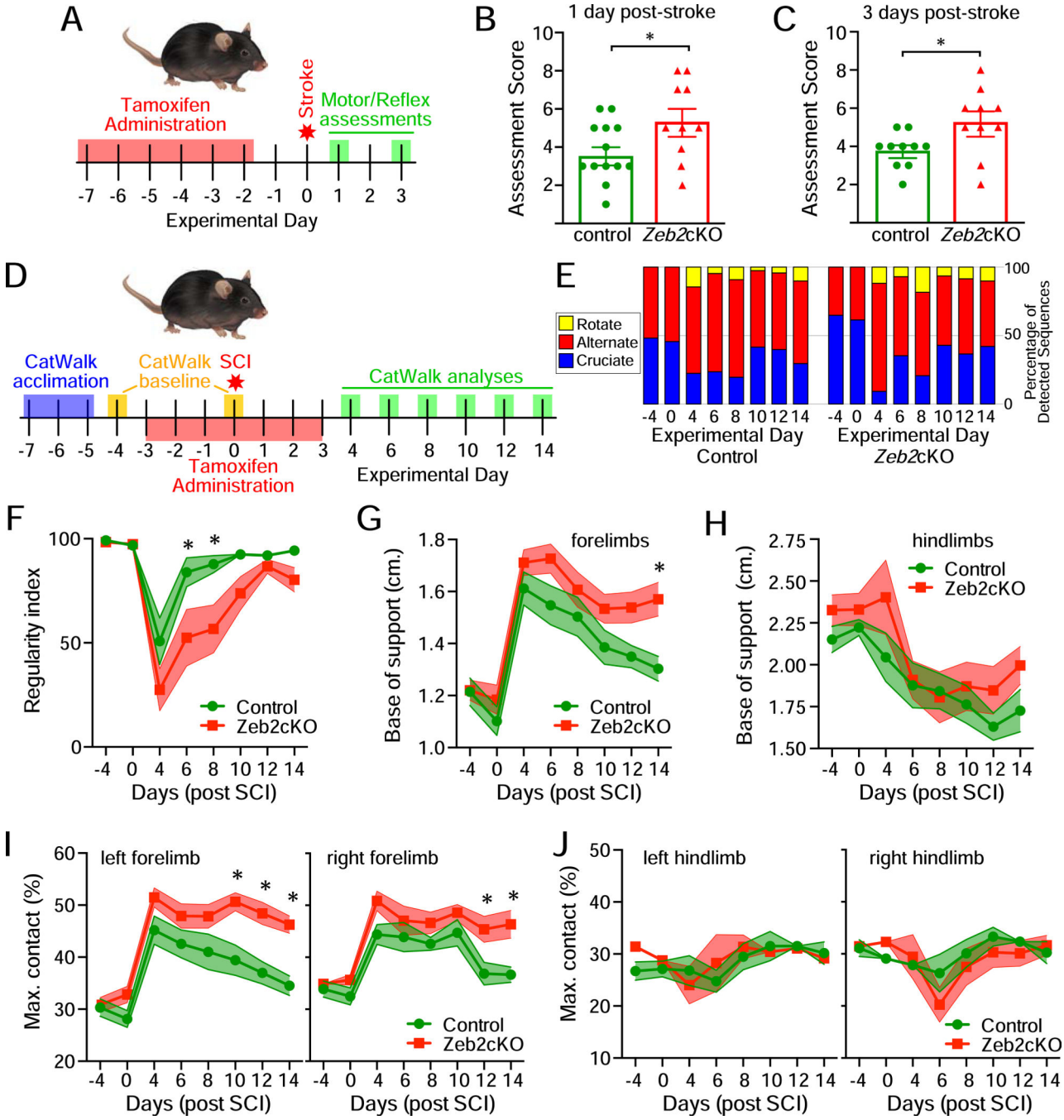

Figure 6.

Delayed recovery of motor function following injury in *Zeb2cKO* mice. **A**, experimental outline for monitoring acute recovery of motor function following ischemic stroke. **B** and **C**, neurological assessments at 1 and 3 days post-stroke, respectively, found impaired recovery of motor and reflex skills in Zeb2c*KO* mice (for B: unpaired Student t test, n=13 for control and n=10 for *Zeb2*cKO, $p<0.05$, power=0.53; for C: unpaired Student t test, n=10 for both genotypes, $p<0.02$, power=0.71). **D**, experimental outline for monitoring acute and sub-acute recovery of motor function following contusive SCI. **E**, step sequence pattern usage in mice

before and after SCI. **F-J**, time course for the regularity index, base of support, and maximum contact area before gait analysis (CatWalk) parameters before and after SCI. Two-way ANOVA with repeated measures, n=9 for control and n=11 for Zeb2*cKO* mice, asterisks indicate $p \leq 0.03$, power=0.99 (F), 0.98 (G), 0.87 (H), 0.99 and 0.98 (I), 0.56 and 0.92 (J). See also Supplemental Figure S6.

KEY RESOURCES TABLE

REAGENT or RESOURCE	SOURCE	IDENTIFIER
Antibodies		
rat anti-CD11b	Abcam	ab8878; RRID:AB_306831
goat anti-CD31	R&D Systems	AF3628; RRID:AB_2161028
rat anti-CD31	BD Biosciences	550274; RRID:AB_393571
goat anti-GFAP	Santa Cruz Biotech	sc-6170; RRID:AB_641021
rabbit anti-GFAP	Dako/Agilent	Z0334; RRID:AB_10013382
mouse anti-OLIG2	Santa Cruz Biotech	sc-48817; RRID:AB_2157550
mouse anti-NEUN	Millipore	MAB377; RRID:AB_2298772
rabbit anti-ZEB2	Seuntjens et al, 2009	N/A
goat anti-ZEB1	Santa Cruz Biotech	sc-10572; RRID:AB_2273177
mouse anti- β-ACTIN	Sigma	A5316; RRID:AB_476743
rabbit anti- β-ACTIN	Sigma	A2066; RRID:AB_476693
Alexa Fluor Plus 594 donkey anti-rabbit	ThermoFisher/Invitrogen	A32754; RRID:AB_2762827
Alexa Fluor Plus 488 donkey anti-rabbit	ThermoFisher/Invitrogen	A32790; RRID:AB_2762833
Alexa Fluor Plus 594 donkey anti-mouse	ThermoFisher/Invitrogen	A32744; RRID:AB_2762826
Alexa Fluor Plus 594 goat anti-rat	ThermoFisher/Invitrogen	A11007; RRID:AB_10561522
Alexa Fluor Plus 594 donkey anti-goat	ThermoFisher/Invitrogen	A32758; RRID:AB_2762828
Alexa Fluor Plus 488 donkey anti-goat	ThermoFisher/Invitrogen	A32814; RRID:AB_2762838
IRDye 800CW goat anti-mouse	Li-Cor	925-32210; RRID:AB_2687825
IRDye 680LT goat anti-rabbit	Li-Cor	925-68021; RRID:AB_2713919
IRDye 680RD donkey anti-goat	Li-Cor	926-68074; RRID:AB_10956736
IRDye 800CW donkey anti-rabbit	Li-Cor	926-32213; RRID:AB_621848
biotinylated goat anti-mouse IgG antibody	Vector Laboratories	BA-9200; RRID:AB_2336171
Chemicals, Peptides, and Recombinant Proteins		
Tamoxifen	Sigma	T5648-5G
ProLong Gold Antifade Mountant with DAPI	ThermoFisher/Invitrogen	P36935
Odyssey blocking buffer	LiCor	927-40100
RNAlater stabilization solution	ThermoFisher/Invitrogen	AM7020
RNAscope protease III reagents	ACDBio	322340
RNAscope target retrieval buffer	ACDBio	322000
Normal goat serum	Sigma	G9023
Diaminobenzidine (DAB) substrate	Sigma	D4293
FITC-conjugated 70 kDa dextran	Sigma	46945-100MG-F
Critical Commercial Assays		
RNeasy mini-prep kit	Qiagen	74104
QIAshredder columns	Qiagen	79654
Superscript III first-strand synthesis kit	ThermoFisher/Invitrogen	18080051
SYBR green PCR master mix	ThermoFisher/Invitrogen	4309155

REAGENT or RESOURCE	SOURCE	IDENTIFIER
Taqman universal master mix	ThermoFisher/Invitrogen	4364341
NE-PER nuclear and cytoplasmic extraction kit	ThermoFisher/Invitrogen	78833
DC assay	BioRad	5000116
RNAScope fluorescent multiplex detection reagent kit	ACDBio	320850
ABC kit	Vector Laboratories	PK-6100; RRID:AB_2336819
Experimental Models: Organisms/Strains		
Mouse: C57BL/6J	The Jackson Laboratory	JAX000664; RRID:IMSR_JAX:000664
Mouse: Gfap-cre^{ERT2}: Tg(GFAP-cre/ERT2)505Fmv	The Jackson Laboratory	JAX012849; RRID:IMSR_JAX:012849
Mouse: Zeb2^{flox}: B6;129(Cg)-Zeb2<tm1.1Yhi>	Riken Institute	RBRC01924; RRID:IMSR_RBRC01924
Oligonucleotides		
Zeb1 forward primer: ACAAGACACCGCCGTCATTT	This paper	N/A
Zeb1 reverse primer: GCAGGTGAGCAACTGGGAAA	This paper	N/A
Zeb2 (Mm00497193_m1)	ThermoFisher	4331182
Zeb2os (Mm01269795_m1)	ThermoFisher	4351372
Gapdh (Mm99999915_g1)	ThermoFisher	4331182
Zeb2os C1 probe for RNAScope	ACDBio	466611
Software and Algorithms		
Prism	GraphPad Software	RRID:SCR_002798
G*Power	Faul et al., 2009	https://www.psychologie.hhu.de/en/research-teams/cognitive-and-industrial-psychology/gpower.html
ImageJ	National Institutes of Health	https://imagej.nih.gov/ij/
Stereo Investigator	MBF Bioscience	RRID:SCR_002526
Neurolucida	MBF Bioscience	RRID:SCR_001775
Axiovision	Zeiss	RRID:SCR_002677
Other		
Infinite Horizons Impactor	Precision Systems & Instrumentation	IH-0400 Impactor
CatWalk XT	Noldus Inc.	N/A
Periflux System Laser-Doppler flowmeter	Perimed AB	PF5010
6-0 teflon-coated monofilament suture for MCAO (5–6mm coating length, 0.25mm diameter)	Doccol Corp.	602556PK10
HybEZ Hybridization System	ACDBio	310010
Odyssey Imaging System	LiCor	N/A
Reactive astrocyte RNA-seq database	Anderson et al., 2016	https://astrocyte.rnaseq.sofroniewlab.neurobio.ucla.edu/homesci
GSEA hallmark epithelial-to-mesenchymal transition (M5930)	GSEA; MSigDB; Univ. California San Diego; Broad Institute	https://www.gsea-msigdb.org/gsea/msigdb/cards/hallmark_epithelial_mesenchymal_transition